HHS Public Access

Author manuscript

Dev Biol. Author manuscript; available in PMC 2022 August 01.

Published in final edited form as:

Dev Biol. 2021 August ; 476: 173–188. doi:10.1016/j.ydbio.2021.03.024.

Altered sacral neural crest development in *Pax3* spina bifida mutants underlies deficits of bladder innervation and function

Karen K. Deal[#1], **Anoop S. Chandrashekar**[#2], **M. Makenzie Beaman**[2], **Meagan C. Branch**[1], **Dennis P. Buehler**[1], **Simon J. Conway**[3], **E. Michelle Southard-Smith**[^,1]

[1]Division of Genetic Medicine, Department of Medicine, Vanderbilt University School of Medicine, Nashville, TN, USA

[2]Vanderbilt University, Nashville, TN, USA

[3]HB Wells Center for Pediatric Research, Indiana University School of Medicine, Indianapolis, IN, USA

[#] These authors contributed equally to this work.

Abstract

Mouse models of Spina bifida (SB) have been instrumental for identifying genes, developmental processes, and environmental factors that influence neurulation and neural tube closure. Beyond the prominent neural tube defects, other aspects of the nervous system can be affected in SB with significant changes in essential bodily functions such as urination. SB patients frequently experience bladder dysfunction and SB fetuses exhibit reduced density of bladder nerves and smooth muscle although the developmental origins of these deficits have not been determined. The *Pax3 Splotch-delayed (Pax3$^{Sp\text{-}d}$)* mouse model of SB is one of a very few mouse SB models that survives to late stages of gestation. Through analysis of *Pax3$^{Sp\text{-}d}$* mutants we sought to define how altered bladder innervation in SB might arise by tracing sacral neural crest (NC) development, pelvic ganglia neuronal differentiation, and assessing bladder nerve fiber density. In *Pax3$^{Sp\text{-}d/Sp\text{-}d}$* fetal mice we observed delayed migration of Sox10+ NC-derived progenitors (NCPs), deficient pelvic ganglia neurogenesis, and reduced density of bladder wall innervation. We further combined NC-specific deletion of *Pax3* with the constitutive *Pax3$^{Sp\text{-}d}$* allele in an effort to generate viable *Pax3* mutants to examine later stages of bladder innervation and postnatal bladder function. Neural crest specific deletion of a *Pax3* flox allele, using a Sox10-cre driver, in combination with a constitutive *Pax3$^{Sp\text{-}d}$* mutation produced postnatal viable offspring that

[^]**Corresponding Author:** Dr. E. Michelle Southard-Smith, Division of Genetic Medicine, Department of Medicine, Vanderbilt University, 2215 Garland Ave, 507 Light Hall, Nashville, TN 37232-0275, michelle.southard-smith@vanderbilt.edu.

Author Contributions

KKD, ASC, and MMB performed experiments, collected data, prepared draft figures and text. MB and DPB performed experiments and collected data. KKD and ASC analyzed data and drafted the manuscript. SJC provided essential resources and reviewed manuscript drafts. EMS[2] conceived the study, acquired funding, directed the project, participated with data analysis, and wrote and edited the manuscript for critical content.

Competing Interests

The authors declare no competing or financial interests.

exhibited altered bladder function as well as reduced bladder wall innervation and altered connectivity between accessory ganglia at the bladder neck. Combined, the results show that *Pax3* plays critical roles within sacral NC that are essential for initiation of neurogenesis and differentiation of autonomic neurons within pelvic ganglia.

Graphical Abstract

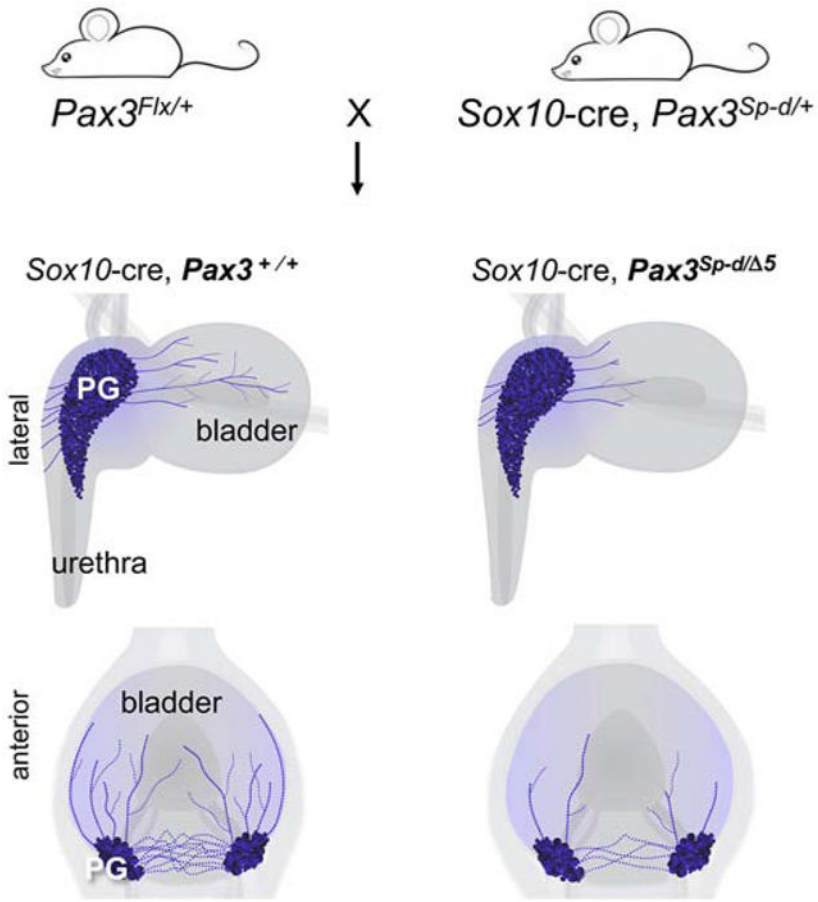

Keywords

sacral neural crest; Pax3; pelvic ganglia; bladder; autonomic nervous system; lower urinary tract

1. Introduction

Spina bifida (SB) is a complex congenital phenotype with both genetic and environmental factors that contribute to severity of the disorder. SB affects an estimated 1 in 1,000 newborns worldwide (Copp et al., 2015). If severe, SB can be lethal before or shortly after birth. In mild SB cases, splaying of the neural tube is limited to the caudal back (a condition called rachischisis) that can be corrected surgically *in utero*. Despite surgical repair of neural tube defects, surviving SB individuals often experience aberrant bladder contractility, called neurogenic bladder, that persists into adulthood (Cass and Spence, 1973; Wiener et al.,

2018). Neurogenic bladder is a general term referring to inappropriate bladder contractility that can range from detrusor overactivity to underactivity. SB is the disorder most frequently associated with pediatric neurogenic bladder. SB patients exhibit reduced innervation of the bladder wall and thinning of the detrusor smooth muscle (Shapiro et al., 1998). To date, the cause of these defects in the SB bladder and the origins of altered bladder contractility are not well understood.

Developmental studies in mouse models of SB have great potential to reveal processes that contribute to disorders of lower urinary tract function such as neurogenic bladder that are common among SB patients. While more than 400 mouse models of SB exist (Bult et al., 2019), only four known models survive to birth. *Pax3 Splotch-delayed (Pax3$^{Sp\text{-}d}$)* is one of these, with neural tube defects generally limited to the caudal spine. Study of *Pax3$^{Sp\text{-}d}$* is advantageous as a single gene model since it can be readily combined with floxed alleles to study gene effects in distinct lineages (Koushik et al., 2002; Olaopa et al., 2011). Because the single base change in the *Pax3$^{Sp\text{-}d}$* allele retains the ability of the Paired box transcription factor to bind DNA and encodes the full-length protein, this allele exhibits a milder phenotype than other complete loss of function *Pax3* mutations (Underhill et al., 1995). *Pax3$^{Sp\text{-}d/Sp\text{-}d}$* embryos survive to later stages of gestation, with some homozygous mutants being present at 18 days post coitus (dpc). This delayed death of *Pax3$^{Sp\text{-}d}$* mutants facilitates analysis of peripheral nervous system development and bladder innervation. *Pax3$^{Sp\text{-}d}$* homozygotes exhibit caudal rachischisis that occurs in some SB patients and these mice also model the bladder wall deficiencies that occur in SB patients (Shinoshima, 2004). Reports of *PAX3* mutations in SB patients (Hol et al., 1995; Lu et al., 2007; Mohd-Zin et al., 2017) provide further rationale for characterizing *Pax3* variants as one avenue to understand developmental mechanisms that contribute to neurogenic bladder.

Pelvic autonomic ganglia originate from sacral neural crest during development (Anderson et al., 2006; Mundell et al., 2012; Wang et al., 2011) and provide autonomic innervation of the bladder. A detailed spatial and temporal timeline of developing bladder innervation has recently been derived by tracing migration of neural crest-derived progenitors (NCPs) that express a fluorescent transgene driven from Sox10 regulatory regions, *Sox10*-H2BVenus (Wiese et al., 2017). These studies show NCPs approach the developing genitourinary sinus by 11.5 dpc in the mouse, where they subsequently aggregate to form pelvic autonomic ganglia flanking either side of the primitive bladder. Within these ganglia NCPs differentiate into sympathetic and parasympathetic neurons that participate in control of bladder contractility and innervate the genitalia and distal colon in adults. By 14.5dpc in the mouse pelvic ganglia neurogenesis is actively ongoing, accompanied by expression of multiple transcription factors that are known to play essential roles in development of the other aspects of the autonomic nervous system, including *Hand2, Hand1, Phox2b*, and *Pax3* (Wiese et al., 2012). Although these neurogenic transcription factors are present throughout late fetal and early postnatal maturation of the pelvic ganglia, to date nothing is known about the factors that participate in generation of the neuronal classes that make up these ganglia in adulthood (Wanigasekara et al., 2003).

Pax3 is a master regulatory gene in NC development that affects diverse processes including cell adhesion (Barber et al., 2002; Lin et al., 2017), migration (Milet et al., 2013),

differentiation (Lin et al., 2017; Milet et al., 2013; Minchin and Hughes, 2008; Monsoro-Burq, 2015), proliferation (Doddrell et al., 2012; Monsoro-Burq, 2015), and survival/apoptosis (Borycki et al., 1999; Zhou et al., 2008). Not only is Pax3 expressed during early phases of NC development, we also observed expression of *Pax3* within developing pelvic ganglia across stages from 14.5dpc to postnatal day 10 (P10) when NCPs are differentiating into neurons (Southard-Smith, 2012; Wiese et al., 2012). Analysis of Pax3 gene functions in mouse and chick have identified important roles for this transcription factor in neurogenesis in multiple aspects of the nervous system including the spinal cord, dorsal root ganglia, and trigeminal ganglia (Dude et al., 2009; Lin et al., 2016; Nakazaki et al., 2008). However, specific roles for *Pax3* in development of pelvic ganglia autonomic neurons and bladder innervation have not previously been examined.

In this report we identify altered development of peripheral innervation in the lower urinary tracts of $Pax3^{Sp\text{-}d}$ mutant mice. By analyzing fluorescent transgenics that label migrating NCPs in homozygous $Pax3^{Sp\text{-}d/Sp\text{-}d}$ mutants combined with NC-specific gene deletion of *Pax3* via floxed alleles we identify several aspects of sacral neural crest development that are disrupted by *Pax3* loss. Specifically, our results show that *Pax3* mutation alters early NPC migration prior to condensation of the pelvic ganglia, reduces overall proliferation within pelvic ganglia, and subsequently alters NPC colonization of the bladder body. We identify a role for *Pax3* in pelvic ganglia neurogenesis and unexpectedly find that *Pax3* mutation can alter neuronal differentiation within the pelvic ganglia. Finally, we observe that *Pax3* mutation alters density of contralateral nerve fibers that connect pelvic ganglia at the level of the bladder neck with males more prominently affected than females. These findings are the first steps towards a more mechanistic understanding of bladder dysfunction in SB patients.

2. Materials and Methods

2.1 Animal husbandry

The Institutional Animal Care and Use Committee at Vanderbilt University Medical Center approved all animal procedures. Mouse strains utilized in our studies included: C57BL/6J.$Pax3^{Sp\text{-}d}$ (Jackson Laboratory Stock Stock #565; MGI:1856174); C57BL6/J.$Pax3^{tm1.1Sjc}$ (hereafter $Pax3^{Flx}$, MGI:2385685); Tg(Sox10-HIST2H2BE/Venus)ASout (hereafter *Sox10*-H2BVenus, MGI:3769269); Tg(Sox10/cre)1Sout (hereafter *Sox10-cre*; MGI:5897484) $B6.Cg\text{-}Gt(ROSA)26Sor^{t14(CAG\text{-}tdTomato/Hze/J}$ (hereafter $Rosa^{Tom}$, Jackson Stock# 7914; RRID: MGI:3809524); . Timed matings were set to obtain staged mouse fetuses, designating the morning of plug formation as 0.5 days post coitum (dpc). The staging of fetuses was confirmed by examination of fore and hind limbs in comparison to published standards (Kaufman, 1995). All animals had access to Rodent Diet 5LOD-irradiated chow (Purina) *ad libitum*. Genotyping was performed to confirm *Sox10*-cre BAC internal and flanking (Sp6 and T7) integrity; Sox10-H2BVenus mice were screened by tissue fluorescence and the integrity of flanking Sp6 and T7 sequences confirmed (Corpening et al, 2011). PCR was used to detect $Pax3^{Sp\text{-}d}$, $Pax3^{Flx}$, and $Pax3^{\Delta 5}$ variant alleles, and all primers and conditions are referenced in Table 1. Embryonic tails were used as a source of genomic DNA in most cases. For analysis of offspring from $Pax3^{flox}$ crosses a small amount of tissue was pinched from the snout (considered predominantly NC-derived) and from the liver (predominantly

non-NC-derived), taking care to prevent cross-contamination by multiple washes of tissue and instruments through 1X PBS. After DNA extraction, PCR was performed according to the protocols in Table 1 and products run on non-denaturing polyacrylamide gels. Gel images were captured following ethidium bromide staining.

Pax3$^{Flx/+}$;*Rosa*$^{Tom/Tom}$ mice were mated with *Sox10-cre*; *Pax3*$^{Sp\text{-}d/+}$ mice to generate *Sox10-cre;Rosa*$^{Tom/+}$;*Pax3*$^{+/+}$, *Sox10-cre*;*Rosa*$^{Tom/+}$;*Pax3*$^{Sp\text{-}d/+}$, *Sox10-cre*;*Rosa*$^{Tom/+}$;*Pax3*$^{+/\Delta 5}$, and *Sox10-cre*;*Rosa*$^{Tom/+}$;*Pax3*$^{Sp\text{-}d/\Delta 5}$ progeny, collectively referred to as "*Pax3* variants;Rosa^{Tom}." Both embryos and weanlings were obtained in a 1:1:1:1 ratio, indicating that NC-specific ablation of Pax3 did not result in intrauterine demise.

2.2 Immunohistochemistry

Harvested tissues were processed for immunohistochemical detection on cryosections using established methods as previously described (Wiese et al., 2017). Antibodies applied for immunohistochemical detection are summarized in Table 2. In order to capture the entirety of the pelvic ganglion, serial sagittal 18μm cryo-sections were generated, beginning at the medial hindlimb, continuing through the bladder, and progressing to the opposite medial hindlimb.

Apoptosis within embryonic pelvic ganglia was detected using the protocol for tissue cryosections in the ApopTag Red In Situ Apoptosis Detection Kit (EMD Millipore Corp., Cat. S7165). Immunohistochemistry with the HuC/D antibody was conducted subsequent to the apoptosis assay.

A modified immunohistochemical protocol was used for analyzing vibratome sections. First, 12.5dpc embryos were fixed overnight in 10% neutral-buffered formalin (Sigma HT501128) at 4°C. Following wash out into 1X PBS, excess liquid was blotted from the embryos, and they were equilibrated at 55°C in 3.5% low-melting point agarose (Invitrogen, 15517-014) for 10min prior to orientation and solidification of the sample at 4°C for 1h. Embryos were serially sectioned (120μm thickness) and visualized under fluorescence to select sections containing pelvic ganglia. Vibratome sections were placed in permeabilization buffer [1xPBS (Sigma P4417) with 0.1% TritonX-100 (Fisher BP151) and 0.5% saponin (Sigma S7900)] overnight at 4°C prior to blocking [1xPBS, 0.1% TX-100, 0.5% saponin, 1% bovine serum albumin (Sigma, A2153), 5% normal donkey serum (Jackson ImmunoResearch, 017-000-121)] overnight at 4°C. Block was removed and Hu C/D antibody (diluted into block solution, see Table 2) added to the sections for 48 h at 4°C without agitation. Sections were then washed 3x 1h each in permeabilization buffer, and TuJ1 antibody added (see Table 2) for an additional 48h at 4°C without agitation. Following copious washing in permeabilization buffer, the sections were incubated in the appropriate secondary antibodies for 3-4h (see Table 2) at RT with gentle rotation. After final washes, the vibratome sections were mounted on slides using Aqua-Poly/Mount (Polysciences, Inc., 18606) and coverslipped prior to imaging by confocal microscopy.

2.3 Post-Natal Whole Mount Tissue Clearing and Immunostaining

Following overnight fixation, flatmount post-natal bladder tissues were washed three times in 1XPBS for 5 minutes each and then incubated in 50% Cubic R1 solution (Susaki et al.,

2014) consisting of 12.5 wt% urea (Sigma), 12.5 wt% N,N,N',N'-tetrakis(2-hydroxypropyl) ethylenediamine (Sigma), and 7.5 wt% TritonX-100 at 37°C for no more than 3 days, changing the solution daily. After permeabilization, tissues were washed three times for an hour each in IHC block at room temperature and then overnight in IHC block at 37°C. The following day, tissues were incubated in primary antibody diluted in IHC block for 3 days at 37°C. Following primary antibody incubation, tissues were washed three times for an hour each in IHC buffer and then incubated in secondary antibody diluted in IHC block for 3 days at 37°C. After incubation in secondary antibody, tissues were rinsed four times for an hour each in IHC buffer and then incubated in 50% Cubic R1 solution overnight at 37°C until tissues cleared, changing solution daily. Once sufficiently cleared, tissues were mounted on slides and cover slipped for microscopy.

2.4 Bright Field and Fluorescent Microscopy

Tissue dissection and bright field and fluorescent imaging of embryos was performed on a Zeiss M2Bio microscope with a Retiga 4000R-F-M-C camera (QImaging) and accompanying software. Fluorescent imaging of wholemount bladders was performed on a Leica DMI6000 B microscope using SimplePCI version 6.6.0.16 imaging software (Hamamatsu). Confocal microscopy was performed on a Zeiss Scanning Microscope LSM510 using a 633 nm laser for imaging Cy5 (649-745 bandpass filter), 543 nm laser for imaging Tomato and Cy3 (560-615 bandpass filter), and a 488 nm laser for imaging Alexa 488 (505-550 bandpass filter) to visualize transgene expression and secondary antibody fluorophores. Images were captured with the Zeiss LSM Image Browser Software, exported as .tiff files, and then tiled in Adobe Photoshop.

2.5 Image Analysis and Quantitation

Quantitation of fetal pelvic ganglia size, neuronal composition, proliferation and apoptosis.—Serial sections (18 μm thickness) of 14.5 dpc pelvic ganglia were generated for the following genotype classes: Sox10-H2BVenus,*Pax3*$^{+/+}$; Sox10H2BVenus,*Pax3*$^{Sp\text{-}d/+}$; Sox10-H2BVenus,*Pax3*$^{Sp\text{-}d/Sp\text{-}d}$; *Sox10*-cre,ROSA^{Tom},*Pax3*$^{+/+}$; *Sox10*-cre,ROSA^{Tom}, *Pax3*$^{Sp\text{-}d/+}$; *Sox10*-cre,ROSA^{Tom},*Pax3*$^{+/\Delta 5}$; *Sox10*-cre,ROSA^{Tom},*Pax3*$^{Sp\text{-}d/Sp\text{-}d}$; and *Sox10*-cre,ROSA^{Tom},*Pax3*$^{Sp\text{-}d/\Delta 5}$. Images were taken from each of three of the largest cross-sections through pelvic ganglia after immunolabeling for HuC/D (pan-neuronal), CGRP (neuronal marker), Ki67 (proliferation), or ApopTag (apoptosis). Area and amount of HuC/D, CGRP, Ki67 and ApopTag staining was quantified within one pelvic ganglia for minimally three independent embryos. Confocal image Z-stacks were compressed into a single project image in ZEISS LSM Image Browser software. Confocal and fluorescent microscope images were converted to 8-bit and opened in ImageJ software (National Institutes of Health). Brightness from image sets were thresholded based on a relative scale of 0 (complete darkness) to 255 (complete saturation) to distinguish true florescence from background using in software tools. Perimeter of pelvic ganglia were defined based on H2BVenus or Tomato signal from single channel image using the free-hand selection tool and selected regions were overlaid onto Hu, CGRP, Ki67, or ApopTag image channels. Area of pixels exceeding the threshold was calculated within the selected region. Scale bars for images at each level of magnification were correlated with pixel size to ensure

all measurement readouts corresponded to metric unit quantities rather than arbitrary pixel values, expressing areas as mm^2.

Fetal bladder wall innervation.—Embryonic bladders (14.5 dpc) from the five *Pax3* variant; $Rosa^{Tom}$ genotypes were cryosectioned in the sagittal plane. Sections that contained both the ureteral insertion (bladder-ureteral reflection, BUR) and the pubis symphysis (PS) were stained by IHC for CGRP and imaged. A line was drawn from the PS to the BUR, setting a boundary that ensured only bladder wall quantitation and avoided signal from the pelvic ganglia. Circular selections with a diameter of 150 pixels were made on the anterior and posterior walls and at the bladder dome (See Fig. 6). Following uniform thresholding, pixel density within the selected regions was measured and quantitated in NIH ImageJ. The bladder length and extent of CGRP innervation was measured as shown in Fig.7A.

Postnatal density of bladder neuronal processes.—*Pax3* variant,$Rosa^{Tom}$ mice were euthanized between postnatal day 35 and 41 (prior to sexual maturity in order to match the age of mice used in the void spot assay below) and bladders dissected. The bladders, with attached accessory ganglia, were cut from the bladder neck to the bladder dome on the posterior aspect, pinned out, and fixed overnight at 4°C in NBF. Following fixation, the bladder tissue was cleared in 50% CUBIC R1, utilizing the protocol and recommended reagents of Muntifering, et al (2018). Following clearing, the bladders were imaged, and a line drawn on each to connect the centers of the two pelvic ganglia, with a subsequent perpendicular line drawn to transect the interganglionic fibers. Pixel density along this perpendicular line was calculated as a measure of interganglionic fiber density (See Fig. 8C). To evaluate the extent of neuronal fiber projections through the bladder wall, a rectangle spanning the width of the pelvic ganglia, oriented parallel to the projections, and extending toward the bladder dome was drawn and divided into quarters. Pixel density was determined along line segments drawn at 25, 50, 75, and 100% of the bladder length as a measurement of fiber density in the bladder wall.

2.6 Spontaneous Void Spot Assay

Spontaneous void spots assays (VSA) were conducted as previously described (Ritter et al., 2017). Briefly, Whatman chromatography paper (Fisher, GE 3030-392) was cut to fit the bottom of each cage then autoclaved. Mice were placed in individual paper-lined cages without food, bedding, or water for a one-hour interval at the same time each day to avoid circadian variability in micturition behavior. Mice were first acclimated under testing conditions for five consecutive days in the same cage and rack position. Following a 2-day rest period, the assay was conducted for three consecutive days and papers collected for analysis. Papers were collected to visualize urine patterns and coded to obscure genotypes. Following colorimetric detection of urine spots with 0.011M ninhydrin (Sigma Aldrich 151173) in 95% ethanol that revealed urine spots as round purple spots, non-urine marks, such as fecal matter, paw prints, and smudges from fur were erased in Adobe Photoshop. The papers were then scanned as black-and-white images and analyzed with the Analyze Particles tool in NIH ImageJ software. The number of individual voids exceeding a threshold of 0.65 mm^2 and the total volume of urine in millimeters squared was quantified for each assay paper. In the case of spot overlap, the region shared was counted twice toward total

area. Total area and total number of void spots were averaged over the three replicate trials collected for each mouse. Scatterplots were generated using the “Stripchart” function in R software.

2.7 Statistical Analysis

Data was compiled and analyzed in MATLAB (2020a). Anderson Darling test for normality and Levene’s test for homogeneity of variance were conducted before applying one-way, two-way, and three-way ANOVA as appropriate. Tukey’s Honestly Significant Differences (HSD) test was used post-hoc to analyze differences between means. Figures were constructed using Prism Graphpad (Version 5). Error bars on graphs represent the standard error of mean (SEM). Statistical significance was set at $p \leq 0.05$.

3. Results

3.1 $Pax3^{Sp\text{-}d/Sp\text{-}d}$ fetal mice model Spina bifida and exhibit aberrant migration of Sox10+ neural crest into bladder body.

Individuals with SB have reduced nerve fiber density of the bladder wall that is thought to predispose patients to neurogenic bladder. As an initial step in understanding the developmental origins of bladder innervation deficits in SB, we used crosses of *Pax3*$^{Sp\text{-}d}$ mice with *Sox10*-H2BVenus transgenics to assess the distribution of migrating NPCs labeled by *Sox10* expression. Offspring from *Sox10*-H2BVenus,*Pax3*$^{Sp\text{-}d/+}$ mice crossed with *Pax3*$^{Sp\text{-}d/+}$ mice included wild type (*Pax3*$^{+/+}$), heterozygous (*Pax3*$^{Sp\text{-}d/+}$), and homozygous (*Pax3*$^{Sp\text{-}d/Sp\text{-}d}$) mutants in normal mendelian ratios at 14.5 dpc. At this stage innervation of lower urinary tract is underway and NCPs have typically colonized the bladder body (Wiese et al., 2017). In contrast to *Pax3*$^{+/+}$ embryos that have smooth spinal curvature extending to the tail (Fig. 1A and 1B), *Pax3*$^{Sp\text{-}d/Sp\text{-}d}$ embryos have prominent caudal rachischisis that is fully penetrant and sometimes accompanied by tail curvature (Fig. 1C and 1D). While a caudal neuropore defect was observed in 100% of *Pax3*$^{Sp\text{-}d/Sp\text{-}d}$ mutants, the severity of rachischisis varied in that the size of the neural tube defect differed among individual embryos. The extent of rachischisis was most often limited to the sacral neural tube; however, in some rare instances (~1 in 20) embryos also exhibited anencephaly. Under fluorescence illumination, *Pax3*$^{+/+}$ embryos exhibit uniformly spaced, symmetrical dorsal root ganglia (DRG) labeled by *Sox10*-H2BVenus transgene expression (Fig. 1B’), whereas *Pax3*$^{Sp\text{-}d/Sp\text{-}d}$ embryos have smaller, misshapen, asymmetrical DRGs immediately rostral to the site of rachischisis, at the level of the defect and distally (Fig. 1D’). In both *Pax3*$^{+/+}$ and *Pax3*$^{Sp\text{-}d/Sp\text{-}d}$ embryos, NCPs populate the hindlimb (via the sciatic nerve) and intestine (compare Fig.1B’ and 1D’).

To view migration of NCPs within the lower urinary tract (LUT) of *Pax3*$^{+/+}$ and *Pax3*$^{Sp\text{-}d/Sp\text{-}d}$ embryos, bladders were micro-dissected and flat-mounted intact for viewing from an anterior perspective. Normally there is extensive colonization of the bladder body by NCPs from prominent clusters of cells that comprise the pelvic ganglia out into the bladder body at 14.5 dpc (Wiese et al., 2017). During this colonization lateral streams of NCPs migrate alongside the blood vessels that flank the bladder body towards the bladder dome while a medial population of progenitors migrates from the anterior bladder neck

ventrally to the bladder dome. In *Pax3*$^{Sp\text{-}d/Sp\text{-}d}$ mutants, lateral migratory streams labeled by *Sox10*-H2BVenus transgene expression were completely absent at 14.5 dpc (n=9). Medial populations of NCPs were present in *Pax3*$^{Sp\text{-}d/Sp\text{-}d}$ bladder; however, these progenitors lacked the typical even spacing seen in wild type bladder, were more closely associated, and in some cases appeared to form continuous chains, all in notable contrast to the more evenly spaced distribution of NCPs in *Pax3*$^{+/+}$ embryos. Efforts to obtain later stages of *Pax3*$^{Sp\text{-}d/Sp\text{-}d}$ mutants for additional analysis to determine whether the absence of lateral NCP migratory streams was due to delayed migration were prevented due to markedly increasing death of fetuses beyond 14.5 dpc.

3.2 At 14.5 dpc Pax3$^{Sp\text{-}d/Sp\text{-}d}$ pelvic ganglia are smaller and exhibit reduced neurogenesis.

Pelvia ganglia are a component of the autonomic nervous system that are essential for bladder muscle relaxation to enable urine storage and initiation of detrusor contraction during micturition. In rodents, these ganglia consist of aggregates of neuronal bodies that during development flank the bladder neck and extend caudally down the sides of the pelvic urethra. Given the prominent role of pelvic ganglia in mediating bladder function and the frequency of neurogenic bladder in SB patients, we examined pelvic ganglia in *Pax3*$^{Sp\text{-}d/Sp\text{-}d}$ embryos. Images of cryosections through the sacral portion of embryos from *Sox10*-H2BVenus,*Pax3*$^{Sp\text{-}d/+}$ crosses revealed that *Pax3*$^{Sp\text{-}d/Sp\text{-}d}$ pelvic ganglia are visibly smaller (Fig.2 A/B). Moreover, when sections were stained for HuC/D, a pan-neuronal marker (King et al., 1999), there was notably less immunolabeling of neuronal cell bodies in *Pax3*$^{Sp\text{-}d/+}$ and *Pax3*$^{Sp\text{-}d/Sp\text{-}d}$ pelvic ganglia. To quantify these differences, we measured the total area of pelvic ganglia and intensity of HuC/D stain for all three genotypes (Fig. 2C-E). *Sox10*-H2BVenus transgene expression marks NCPs and differentiating glial cells and is a ready means to establish the location and borders of the pelvic ganglion. As NCPs differentiate towards a neuronal fate and upregulate HuC/D, Sox10 expression is down-regulated while increasing HuC/D signal provides a proxy for pelvic ganglia neurogenesis (Wiese et al., 2012). The perimeter of pelvic ganglia sections was outlined on the basis of *Sox10*-H2BVenus transgene expression and used to quantify the total area across multiple biological replicates in each genotype class. This analysis confirmed that the size of pelvic ganglia for *Pax3*$^{Sp\text{-}d/Sp\text{-}d}$ mutants and *Pax3*$^{Sp\text{-}d/+}$ heterozygotes was significantly smaller relative to littermate controls (n=8 for each genotype class; Fig. 2C). Moreover, the area and intensity of HuC/D stain, a proxy for neuronal fate commitment, was dramatically reduced (p<0.0001) for *Pax3*$^{Sp\text{-}d/Sp\text{-}d}$ mutants compared to wildtype and heterozygous littermates (Fig. 2D). When the amount of HuC/D immunolabeling was normalized to the area of the pelvic ganglia for each genotype class, we observed significantly reduced pelvic ganglia neurogenesis among *Pax3*$^{Sp\text{-}d/Sp\text{-}d}$ embryos (Fig. 2E).

3.3 Proliferation is reduced within Pax3$^{Sp\text{-}d/Sp\text{-}d}$ pelvic ganglia while apoptosis is unchanged.

The first NCPs that populate the anlagen of the pelvic ganglion aggregate within tight clusters adjacent to the future bladder neck and undergo a marked increase in cell numbers between 12.5-14.5 dpc (Wiese et al., 2017). Given the reduced numbers of neurons within the *Pax3*$^{Sp\text{-}d/Sp\text{-}d}$ pelvic ganglia and the known role of Pax3 in regulating proliferation of

early NC and NC derivatives such as Schwann cells and sensory neurons (Doddrell et al., 2012; Koblar et al., 1999; Monsoro-Burq, 2015), we examined the proliferation of cells within developing pelvic ganglia for these mutants. Staining for Ki67, a prototypical cell cycle marker expressed by proliferating cells, concurrent with HuC/D immunolabeling was used to identify proliferating cells within the pelvic ganglia. Mitotic cells (Ki67+) were observed in pelvic ganglia of all three genotypes as would be expected given the rapid proliferation of cells within tissues during organogenesis. We expected and did observe co-localization of Ki67 with nuclear labeling by the *Sox10*-H2BVenus transgene for those NCPs that were actively proliferating within the pelvic ganglia (Fig. 3). In addition, we were surprised to see many HuC/D+ cells within the pelvic ganglia that were strongly Ki67+ and yet were not expressing *Sox10*-H2BVenus (Fig. 3B). This observation indicates that differentiating neurons, which have down-regulated Sox10 within the pelvic ganglia, are actively dividing. To assess the overall rate of proliferation within the developing pelvic ganglion for both Sox10+ NCPs and HuC/D+ differentiating neurons, we quantified the intensity of Ki67 immunolabeling as a percentage of total pelvic ganglia area. Our analysis identified significant differences in proliferating cells, either YFP+ or HuC/D+, for $Pax3^{Sp\text{-}d/Sp\text{-}d}$ and $Pax3^{Sp\text{-}d/+}$ relative to wild type $Pax3^{+/+}$ littermates processed in parallel.

Reduced *Pax3* expression leads to lineage specific apoptosis in somites during development (Zhou et al., 2008). To our knowledge, apoptosis within $Pax3^{Sp\text{-}d/Sp\text{-}d}$ mutants has not been reported. We assessed apoptosis as a developmental mechanism that might contribute to the reduced numbers of neurons within $Pax3^{Sp\text{-}d/Sp\text{-}d}$ pelvic ganglia, by ApopTag® labeling, a modified TUNEL assay that fluorescently labels DNA nicks in dying cells (Li et al., 1995). Negligible levels of apoptosis were detected in $Pax3^{+/+}$, $Pax3^{Sp\text{-}d/+}$, and $Pax3^{Sp\text{-}d/Sp\text{-}d}$ pelvic ganglia and no differences were observed among the genotype classes despite detecting normal levels of apoptosis in developing dorsal root ganglia (DRG) (data not shown). These findings indicate that at the stage when bladder innervation is underway and NC progenitors have colonized the urogenital sinus, apoptosis within pelvic ganglia is not a primary factor in the reduced numbers of neurons in $Pax3^{Sp\text{-}d/Sp\text{-}d}$ mutants.

3.4 $Pax3^{Sp\text{-}d/Sp\text{-}d}$ NPCs colonize the urogenital sinus at 12.5 dpc and fail to initiate timely neurogenesis.

Prior studies investigating development of parasympathetic and sympathetic neurons in cranial and trunk regions of the embryo have shown that bi-potent progenitors migrate along nerve processes to reach ganglia anlagen and then differentiate to form neurons and glia (Dyachuk et al., 2014; Espinosa-Medina et al., 2014). To evaluate the effects of *Pax3* mutation on the initial colonization of the urogenital sinus we, examined migration of NPCs on the basis of *Sox10*-H2BVenus transgene expression in parallel with TuJ1 immunostaining to label developing nerve fibers and localization of HuC/D to mark differentiating neurons in vibratome sections (Fig. 4). At 12.5dpc in both $Pax3^{+/+}$ and $Pax3^{Sp\text{-}d/Sp\text{-}d}$ embryos, nerve fibers had entered the base of the genital tubercle and extended beyond the anterior cluster of NPCs towards the distal end of the genital tubercle marking the formation of the pudenal nerve. Prominent HuC/D immunolabeling was observed within the aggregates of NPCs at the base of the genital tubercle in $Pax3^{+/+}$ embryos at 12.5 dpc (Fig. 4A upper panels and 4B). However, at the comparable location in $Pax3^{Sp\text{-}d/Sp\text{-}d}$ embryos HuC/D labeling was

completely absent at this stage (Fig. 4A, lower panels and 4B'). In wild type *Pax3*$^{+/+}$ embryos, small numbers of HuC/D-positive neuronal progenitors were detectable migrating upwards along TuJ1+ fibers from the main NPC aggregate at the base of the genital tubercle to the location of the pelvic ganglia anlagen adjacent to the blood vessels that flank the developing bladder (arrow in Fig. 4A). We did not detect migrating progenitors at this location in *Pax3*$^{Sp\text{-}d/Sp\text{-}d}$ embryos despite the presence of TuJ1+ nerve fibers. HuC/D-positive progenitors were readily detected along nerve fibers extending from dorsal root ganglia at sacral levels for both *Pax3*$^{+/+}$ and *Pax3*$^{Sp\text{-}d/Sp\text{-}d}$ embryos (Fig. 4C and 4C'). The absence of HuC/D immunostaining within the aggregate of *Sox10*-H2BVenus labeled NPCs (compare upper and lower panels in Fig. 4A) suggests that activity of the normal Pax3 isoform is required to initiate neurogenesis in pelvic ganglion progenitors. The reduced amount of HuC/D labeling observed later at 14.5dpc within pelvic ganglia of *Pax3*$^{Sp\text{-}d/Sp\text{-}d}$ embryos (see Fig. 2) indicates that these mutants do go on to form neurons within this ganglion, albeit at a marked delay, and supports an essential role for *Pax3* in this process.

3.5 NC-specific deletion of Pax3 has minimal effect on pelvic ganglia neuronal lineages at 14.5dpc despite altered composition of pelvic ganglia in Pax3$^{Sp\text{-}d/Sp\text{-}d}$ mutants

Pax3 is widely expressed in development having been detected in early neural folds, NC emigrating from the neural tube, and forming somites (Engleka et al., 2005; Goulding et al., 1991). We previously had also detected *Pax3* by whole mount *in situ* hybridization and reverse transcription PCR within isolated pelvic ganglia at 14.5 dpc with sustained expression of the gene to postnatal day 10 (P10) (Southard-Smith, 2012; Wiese et al., 2012). To examine whether NC-specific functions of *Pax3* contribute to the bladder innervation deficiencies seen in the *Pax3*$^{Sp\text{-}d}$ SB mouse model, we crossed a conditional allele of *Pax3* (*Pax3*^{flox}), with a NC cre driver (*Sox10*-cre; (Deal et al., 2020)) to selectively ablate *Pax3* from NC derivatives. This *Sox10*-cre line lineage labels derivatives of migrating NC including NCPs that colonize the LUT, and comprehensively labels pelvic ganglia neurons in contrast to the canonical *Wnt1*-cre line that that less efficiently labels sacral NC derivatives (Deal et al., 2020). We established crosses that removed exon 5 of Pax3 (*Pax3*$^{\Delta 5}$) as previously described (Koushik et al., 2002) in the context of the *Pax3*$^{Sp\text{-}d}$ allele (Fig. 5). Inclusion of the Ai14 *ROSA*^{Tom} reporter (Madisen et al., 2010) in these crosses generated concurrent permanent labeling of all NC lineages so that the entirety of the developing pelvic ganglia was labeled as well as all neuronal fibers in the bladder wall based on tdTomato fluorescence.

Based on observed changes in *Pax3* mRNA levels across stages of fetal pelvic ganglia development (Wiese et al., 2012) and the pronounced effect of gene loss on differentiation of other NC-derived lineages in development (Doddrell et al., 2012; Milet et al., 2013; Minchin and Hughes, 2008), we postulated that loss of Pax3 might disrupt distinct lineages within the pelvic ganglia. Subsequent immunolabeling of neurons expressing CGRP, identified absence of neurons expressing this gene in *Pax3*$^{S\text{-}pd/Sp\text{-}d}$ mutant embryos at 14.5dpc (Fig. 6A). CGRP is a canonical sensory neuron marker that is also transiently expressed within cell bodies of developing pelvic ganglia neurons in fetal stages although it is extinguished by P7 (Smith-Anttila et al., 2021). Absence of any CGRP expression in *Pax3*$^{S\text{-}pd/Sp\text{-}d}$ mutants suggests that normal activity of the *Pax3* transcription factor is required for appropriate

progression of neuronal differentiation. We subsequently examined expression of Tyrosine Hydroxylase (TH) in *Pax3*$^{S\text{-}pd/Sp\text{-}d}$ embryos at the same stage, as this marker is widely used to assess development of noradrenergic neurons (Fig. 7). In *Pax3*$^{S\text{-}pd/Sp\text{-}d}$ mutants at 14.5 dpc, TH immunolabeling was present, although like HuC/D it was reduced by comparison to wild type littermates. These findings suggest that Pax3 function is necessary for some but not all aspects of neuronal differentiation within the pelvic ganglia.

In contrast to the dramatic open neural tube defects observed in *Pax3*$^{S\text{-}pd/Sp\text{-}d}$ mutant embryos, *Pax3*$^{Sp\text{-}d/\Delta 5}$ mutant offspring that carried NC-specific deletion of *Pax3* showed no evidence of rachischisis among any of the resulting embryos (n>20). Upon immunolabeling of total neurons and neuron subtypes in pelvic ganglia *Pax3*$^{Sp\text{-}d/\Delta 5}$ mutant embryos, both HuC/D and CGRP expression were present (Fig. 6A). We quantitatively assessed the overall size of pelvic ganglia in all genotype classes by tracing the perimeter of Tomato+ pelvic ganglia sections from 14.5 dpc embryos (Fig. 6B). The average area of NC derivatives in the pelvic ganglia of *Pax3*$^{Sp\text{-}d/Sp\text{-}d}$ mutants was smaller when measured on the basis of tdTomato fluorescence, although not statistically significant when compared with littermate controls. Pelvic ganglia from conditional cross progeny, *Pax3*$^{\Delta 5/+}$ and *Pax3*$^{Sp\text{-}d/\Delta 5}$, at 14.5 dpc were not appreciably smaller than other genotypes classes.

Distinct neuron subtypes are present within fetal mouse pelvic ganglia by 14.5 dpc (Ritter et al., 2017). To assess the effect of NC-specific deletion of *Pax3* on subtypes of neurons within pelvic ganglia, sections from *Pax3*$^{Sp\text{-}d/\Delta 5}$ mutant embryos were stained with HuC/D in parallel with littermate controls and *Pax3*$^{Sp\text{-}d/Sp\text{-}d}$ mutants. We did not observe significant reductions in the amount of total HuC/D labeling or neurons expressing CGRP among *Pax3*$^{Sp\text{-}d/\Delta 5}$ pelvic ganglia despite the pronounced effect seen in *Pax3*$^{Sp\text{-}d/Sp\text{-}d}$ fetal mice (Fig. 6C, 6D). Overall, our results show that there is a pronounced effect of the *Pax3*$^{Sp\text{-}d}$ allele on neuronal differentiation within pelvic ganglia at 14.5 dpc, although no significant differences were detectable for NC-specific ablation of *Pax3* at this stage.

3.5 Bladder wall innervation varies significantly among Pax3 mutants in fetal stages

SB patients show loss of nerve fibers and smooth muscle in the lower genitourinary tract (Shapiro et al., 1998). To determine whether *Pax3* constitutive (*Sp-d*) and conditional (*Δ5*) alleles recapitulate this feature of SB, we assessed bladder wall innervation among *Pax3* fetal mutants by imaging density of tdTomato (all nerve fibers and glial cells), HuC/D, and CGRP+ labeled nerve fibers at 14.5 dpc. Nerve fiber density was quantified as previously described for the anterior and posterior bladder neck and the bladder dome (Ritter et al., 2017) Fig. 8A). At 14.5 dpc no HuC/D staining was detected in the bladder body. Moreover, Tomato+ NC-derivatives and CGRP+ fibers at this stage were consistently absent from the bladder dome. In the anterior bladder CGRP+ nerve fiber density for *Pax3*$^{\Delta 5/+}$ heterozygotes trended lower; however, only *Pax3*$^{Sp\text{-}d/Sp\text{-}d}$ mutants showed significantly reduced density of CGRP+ nerve fibers in this region compared to wild types (Fig. 8B). No differences were detected for total nerve fiber density measured on the basis of Tomato fluorescence. And, density of CGRP+ fibers in the posterior bladder did not differ among any of the genotype classes. We also quantified the extent of bladder wall innervation determined as a proportion of the furthest CGRP nerve fibers detected in the anterior bladder compared to total bladder

length (Fig. 8C). This measure allowed us to determine which *Pax3* variants exhibited reduced migration of nerve processes towards the bladder dome relative to $Pax3^{+/+}$. Again, we observed lower trends for $Pax3^{\Delta 5/+}$ heterozygotes; however, only $Pax3^{Sp\text{-}d/Sp\text{-}d}$ mutants showed significant loss of CGRP+ nerve fibers along the length of the bladder at 14.5dpc. Both pelvic ganglia and dorsal root ganglia neurons express CGRP at this stage of development. Our results suggest that dorsal root ganglia nerve terminals are also affected in the $Pax3^{Sp\text{-}d/Sp\text{-}d}$ mutant. In normal development CGRP would label both sensory nerve fibers coming from dorsal root ganglia neurons and neuronal cell bodies/processes of pelvic ganglia. However, there is complete absence of CGRP+ nerve fibers in $Pax3^{Sp\text{-}d/Sp\text{-}d}$ mutant bladders concurrent with the absence of CGRP expression in pelvic ganglia at 14.5dpc. These findings demonstrate that $Pax3^{Sp\text{-}d/Sp\text{-}d}$ mice model deficiencies of the nerve fibers seen in human fetuses.

3.6 Postnatal urination patterns are altered in compound heterozygous Pax3 mutants with NC-specific loss of Pax3

Survival of $Pax3^{Sp\text{-}d/Sp\text{-}d}$ mutants to 19 dpc has been reported in the literature (Dickie, 1964); however, perinatal lethality of $Pax3^{Sp\text{-}d/Sp\text{-}d}$ mutants prohibits analysis of postnatal bladder innervation and functionality at later stages. A SB model that survives postnatally as the bladder and neural connections that control urination mature would be particularly valuable to investigators studying mechanisms of pediatric bladder dysfunction. Because compound mutants carrying the constitutive $Pax3^{Sp\text{-}d}$ mutation in combination with the NC-specific *Δ5* allele exhibited mild phenotypes during fetal stages that were not significantly different from $Pax3^{+/+}$ littermates, we tested the possibility that $Pax3^{Sp\text{-}d/\Delta 5}$ mutants would survive postnatally by allowing litters from crosses of $Pax3^{flox}$,$ROSA^{Tom/Tom}$ with $Pax3^{Sp\text{-}d/+}$,*Sox10*-cre mice to be born. We found that $Pax3^{Sp\text{-}d/\Delta 5}$ mutants consistently survived to six weeks of age, although they were significantly smaller relative to their littermates and exhibited extensive spotting (Fig. 9), consistent with the known role of Pax3 in melanogenesis (Hauswirth et al., 2019; Hornyak et al., 2001; Kubic et al., 2008). The compound mutants did exhibit micrognathia and misalignment of their teeth that may have contributed to their smaller size. No spinal malformations were detected among postnatal $Pax3^{Sp\text{-}d/\Delta 5}$ mice by skeletal staining (data not shown) consistent with deletion of *Pax3* in these mice being restricted to NC lineages.

While neuronal differentiation in pelvic ganglia of $Pax3^{Sp\text{-}d/\Delta 5}$ mutants at 14.5dpc was not dramatically altered based on staining for the two neuronal markers (HuC/D and CGRP) that were assayed, we reasoned that NC-specific ablation of *Pax3* might alter later stages of pelvic ganglia development given the previously documented transcription of *Pax3* in pelvic ganglia from 14.5dpc to P10 (Wiese et al., 2012). Thus, deletion of *Pax3* from NPCs that colonize the developing lower urinary tract might affect later stages of pelvic ganglia maturation and subsequent bladder innervation when the gene is expressed. We evaluated bladder function of $Pax3^{Sp\text{-}d/\Delta 5}$ mice using a spontaneous void spot (VSA) assay that has been shown in prior studies to be a reliable assessment of micturition in mice (Bjorling et al., 2015; Keil et al., 2016; Yu et al., 2014). In 1-hour assessments measured for 4-week old mice across 3 consecutive days, we recorded the largest void spot, which is also referred to as the primary void spot and is typically the initial release of urine in mice (Rajandram et al.,

2016), the total area of urine, and the total number of urine spots. The largest void (primary) for male *Pax3*$^{Sp\text{-}d/\Delta 5}$ mutants was significantly less ($p \leq 0.005$) than that of *Pax3*$^{+/+}$ and *Pax3*$^{\Delta 5/+}$ littermates (Fig. 10). In addition, the total area of urine released over the course of the assay was also less for male *Pax3*$^{Sp\text{-}d/\Delta 5}$ mutants relative to littermate *Pax3*$^{+/+}$ mice tested in parallel (Fig. 10B, $p \leq 0.05$). There was no significant difference in the total number of voids quantified across all male genotypes and no significant difference between *Pax3* variants compared to wild type littermates for females (Fig. 10C). These findings indicate that NC-specific deletion of *Pax3* in *Pax3*$^{Sp\text{-}d/\Delta 5}$ mutants alters bladder function leading to less initial release of urine and reduced overall urine release in males.

3.8 Postnatal bladder innervation and interganglionic connectivity of accessory pelvic ganglia is deficient among Pax3$^{Sp\text{-}d/\Delta 5}$ mutants

NC-specific deletion of *Pax3* has the potential to impact neuronal and glial cells of the peripheral nervous system that originate from NCPs during development. Given the altered voiding patterns detected in *Pax3*$^{Sp\text{-}d/\Delta 5}$ mutants, we assessed density of bladder innervation by visualizing Tomato fluorescence in postnatal bladders generated by ROSA^{Tom} labeling as a function of *Sox10*-cre. Lower urinary tract tissues including the bladder and urethra were dissected intact from *Pax3*$^{Sp\text{-}d/\Delta 5}$ mutants and littermates, bisected along the ventral surface, pinned out flat, then cleared to facilitate imaging of Tomato+ nerve fibers. Despite the altered voiding function detected in *Pax3*$^{Sp\text{-}d/\Delta 5}$ mutants, we observed no visible alterations of the bladder wall based on morphology, either hypertrophy or distension, at the time of tissue collection. Density of innervation was assessed by imaging tdTomato fluorescence, a surrogate for all nerve fiber types since the *Sox10*-cre line is expressed in both dorsal root and pelvic ganglia neurons. Density of innervation was quantified from an anterior perspective by measuring intensity of Tomato fluorescence at positions equivalent to 25, 50, 75, and 100% increments of the total bladder length from bladder neck to the bladder dome based on an anchor line drawn between accessory ganglia at the bladder neck (Fig. 11). As expected, based on initial colonization of the bladder by NCPs during development and the location of accessory ganglia that are tightly adherent to the bladder neck (Arellano et al., 2019; Wiese et al., 2017), nerve fiber density was highest near the bladder neck and decreased towards the bladder dome. Because fetal development beyond 15.5 dpc is subjected to differences in hormonal levels based on the sex of the embryo, we evaluated males and females separately in postnatal assays. We found that all male *Pax3* mutant genotypes exhibited significantly diminished bladder wall innervation compared to wild type *Pax*$^{+/+}$ littermates ($p<0.05$; Fig. 11B). Among females, only *Pax3*$^{Sp\text{-}d/\Delta 5}$ mutants had significantly reduced nerve fiber density in the bladder wall ($p<0.05$). During the course of our analysis, we observed what appeared to be differences in the connecting commissural nerve fibers that run between the left and right accessory ganglia that are embedded in the bladder neck wall (Arellano et al., 2019). To assess density of commissural nerve fibers between these accessory ganglia in *Pax3* variants, we quantified the intensity of Tomato fluorescence in this region along a line centered between the accessory ganglia that extended from the most ventral interganglionic fiber to the most dorsal fiber (Fig. 11C). This analysis identified significant differences in interganglionic fiber density between males and females for each genotype ($p<0.05$). Significant differences in fiber density were also discovered between genotype classes (Fig. 11D, 11D'). Among males, average interganglionic

connectivity for *Pax3*$^{+/+}$ was 49.2% with *Pax3* variants displaying reduced fiber density across all genotypes (*Pax3*$^{\Delta 5/+}$ 32.6%; *Pax3*$^{Spd/+}$ 36.0%; *Pax3*$^{Sp\text{-}d/\Delta 5}$ 23.3%). Similar trends were present in females where average interganglionic fiber connectivity for *Pax3*$^{+/+}$ was 15.4% with *Pax3* variants displaying reduced fiber density across all genotypes (*Pax3*$^{\Delta 5/+}$ 10.8% ; *Pax3*$^{Spd/+}$ 14.2%; *Pax3*$^{Sp\text{-}d/\Delta 5}$ 2.91%), although only *Pax3*$^{Spd/d5}$ females were significant for this measure. These findings demonstrate that LUT innervation patterns are altered in both male and female *Pax3*$^{Sp\text{-}d/\Delta 5}$ mutants, although only males show significantly altered urination patterns in VSA.

4. Discussion

Based on the expression of *Pax3* during neurogenic phases in the pelvic ganglia and the prominent roles for this transcription factor in other NC-derived lineages, we undertook analysis of *Pax3* mutants to assess potential roles for this gene in development of bladder innervation. Through analysis of a constitutive *Pax3*$^{Sp\text{-}d/Sp\text{-}d}$ mutant we have determined that normal *Pax3* function is required for timely initiation of autonomic neurogenesis within the pelvic ganglia and appropriate progression of neuronal differentiation (as evidenced by reduction of Hu and lack of CGRP expression). Our results show that analogous to other aspects of peripheral nervous system development (Dyachuk et al., 2014; Espinosa-Medina et al., 2014), sacral NCPs migrate into the urogenital system along developing nerve fibers. Using a conditional NC-specific compound mutant *Pax3*$^{Sp\text{-}d/\Delta 5}$ we determined that Pax3 is required within NC lineages to generate normal bladder innervation density and connectivity of neurons between opposing accessory ganglia located at the bladder neck (Fig. 11).

There are many causes that lead to the characteristic open neural tube that defines SB. Previously more than 200 mouse models of SB have been reviewed for their impact on neural tube closure (Harris and Juriloff, 2010) and currently there are more than 460 genes in the Mouse Genome Database that are associated with disease term Spina bifida (Bult et al., 2019). *Pax3* is only one gene that has been identified among SB patients. Whether other mouse SB models exhibit similar alterations in development of lower urinary tract innervation remains to be seen. Given the prevalence of bladder dysfunction among SB individuals and the challenges associated with their urological management (Snow-Lisy et al., 2015), gaining additional insights into the causes of SB bladder dysfunction is worthwhile. Of interest is the finding that the *Pax3*$^{Sp\text{-}d/\Delta 5}$ mice we generated lacked neural tube defects and yet exhibited alterations in bladder innervation. Thus, study of genes that participate in development of sacral NC in general may be generally informative for urologists seeking to treat pediatric bladder disorders that arise from innervation deficits.

The majority of *Pax3* alleles are not viable due the central role of this gene in many biological pathways. *Pax3*$^{Sp\text{-}d}$ is unique in that homozygous mutants are viable to later stages of gestation, 14.5 dpc in our colony, and thus permit analyses of later processes in development that are otherwise not feasible due to early fetal death. Analysis of the *Pax3*$^{Sp\text{-}d/Sp\text{-}d}$ SB model revealed that LUT innervation defects in these mutants arise from multiple developmental processes. We observed deficits in initial NPC colonization of the bladder body based on fluorescence of individual cells labeled by the *Sox10*-YFP transgene (Fig. 1), reduced proliferation of NCPs within pelvic ganglia (Fig. 3), altered neuronal

differentiation of pelvic ganglia neurons (Figs. 4, 6, and 7), and reduced density of nerve fibers in the bladder wall (Figs. 8 and 11). The absence of migration of lateral migratory streams within the bladder body of *Pax3*$^{Sp\text{-}d/Sp\text{-}d}$ mutants was particularly interesting and suggests that this migration is distinct from the medial migration that occurs later in the bladder. We attempted to evaluate later stages of development for *Pax3*$^{Sp\text{-}d/Sp\text{-}d}$ mutants to discern whether the absence of lateral migrating NCPs was a result of delayed migration or failure of NCPs to exit the pelvic ganglia. However, due to a severe decline in viability of *Pax3*$^{Sp\text{-}d/Sp\text{-}d}$ mutants beyond 14.5 dpc in the *Pax3*$^{Sp\text{-}d}$ line that we maintain as a congenic on C57BL/6J background, we were unable to examine these possibilities. The fact that the medial streams of migratory NCPs in the bladder actually form in the *Pax3*$^{Sp\text{-}d/Sp\text{-}d}$ suggests that progenitors are present and capable of responding to environmental cues in the bladder body. It may be that the somitic defects in *Pax3*$^{Sp\text{-}d/Sp\text{-}d}$ mutants led to changes in the bladder wall such that loss of a signal that promotes migration out into the bladder was lacking along the lateral pathway. Further analysis of Pax3 conditional mutants using somite-specific Cre lines that permit deletion of Pax3 specifically in the somite could be used to address this possibility in the future.

Pax3 functions in generation of dorsal root sensory neurons (Koblar et al., 1999) so disruption of general neurogenesis in pelvic ganglia detected as a loss of overall HuC/D staining in pelvic ganglia of *Pax3*$^{Sp\text{-}d/Sp\text{-}d}$ mutants was not surprising given the prominent expression of Pax3 in these ganglia mid-gestation (www.GUDMAP.org, Image ID NFEGC; Wiese et al., 2012). However, complete absence of CGRP labeling among neuronal cell bodies of pelvic ganglia neurons in *Pax3*$^{Sp\text{-}d/Sp\text{-}d}$ mutants was an unexpected finding. CGRP labeling of pelvic ganglia neuronal cell bodies is prominent in wild type fetal mice at 14.5dpc (Fig. 6) and other groups have shown that this expression is lost from pelvic ganglia neurons between 18.5dpc and P7 (Smith-Anttila et al., 2021). Whether transient CGRP expression within pelvic ganglia neurons occurs within a specific neuronal subtype or is a broader phenomenon that occurs among all pelvic ganglia neurons as they differentiate remains to be seen. It is possible that Pax3 may have a role in specifying distinct types of autonomic neurons within the pelvic ganglia. However, future analysis with fate-mapping approaches or trajectory studies that examine transcriptional changes in developing pelvic ganglia neurons over time will be needed to comprehensively assess alterations that result from *Pax3* deficiency.

The phenotypes we detected in *Pax3*$^{Sp\text{-}d/\Delta 5}$ mutants, where *Pax3* was ablated from Sox10+ neural crest lineages, were milder than in the constitutive *Pax3*$^{Sp\text{-}d/Sp\text{-}d}$ mutants, particularly at mid-gestation. At 14.5pdc HuC/D levels in pelvic ganglia of *Pax3*$^{Sp\text{-}d/\Delta 5}$ fetal mice were not significantly different from wild type littermates and density of nerve fibers in the bladder wall at this stage only trended towards significance (Fig. 6). However, postnatally *Pax3*$^{Sp\text{-}d/\Delta 5}$ mice exhibited altered urination patterns, reduced levels of bladder innervation, and reduced density of contralateral nerve fibers that connect the accessory ganglia located at the bladder neck (Fig. 11). The difference in phenotype of the *Pax3*$^{Sp\text{-}d/\Delta 5}$ mutants in fetal versus postnatal stages is likely to be the result of two factors. First, the timing of *Pax3* expression in the forming pelvic ganglia is likely an important aspect. Pax3 is barely detectable at 14.5dpc by RT-PCR while transcripts are detected much more readily at 15.5dpc and are sustained through to P10 (Wiese et al., 2012). Second, the timing between

initiation of *Sox10*-cre transgene expression, excision of the *Pax3* flox construct, and decay of wild type Pax3 protein may play a role so that sufficient residual Pax3 protein is present within early migrating NPCs allowing their arrival and initial differentiation within the pelvic ganglia to proceed normally. Subsequently, beyond 14.5 dpc as the pelvic ganglia composition diversifies and autonomic neurons would be making connections, levels of Pax3 would have declined in $Pax3^{Sp\text{-}d/\Delta 5}$ mice. Importantly, the alterations we document in $Pax3^{Sp\text{-}d/\Delta 5}$ mutants are consistent with a later role of Pax3 in pelvic ganglia after NCPs arrive in the anlagen and begin to differentiate into mature neuron types and form connections. Future analysis of $Pax3^{Sp\text{-}d/\Delta 5}$ pelvic ganglia composition through single cell transcriptional profiling will allow a comprehensive assessment of how *Pax3* regulates neuronal differentiation independent of current limitations due to immunohistochemical reagents.

Our analysis of sacral NCP migration identifies a previously unrecognized subtlety in the spatial routing of these progenitors to the site of the pelvic ganglia anlagen medial to the blood vessels between which the future bladder mesenchyme develops. In wild type embryos, NCPs that have initiated HuC/D expression migrate from the initial copious aggregate at the base of the genital tubercle up towards the maturing bladder mesenchyme along TuJ1+ nerve fibers (arrow, Fig. 4A upper panels). We have not observed the same migration in $Pax3^{Sp\text{-}d/Sp\text{-}d}$ mutant embryos at this stage. Eventually even $Pax3^{Sp\text{-}d/Sp\text{-}d}$ NCPs arrive at the pelvic ganglia anlagen flanking the bladder neck as they are visible at 14.5 dpc (Figs. 1, 2, and 3). Whether this difference is due to differences in the TuJ1+ fibers along which the cells migrate, that appear thicker and more “ropey” in mutants, or differences in expression within the mesenchyme that attracts the nerve terminals and accompanying neural progenitors to the condensation site of the pelvic ganglia remains to be determined.

Pax3 is a NC specifier that is required for development of NC and is subsequently down-regulated in many lineages (Meulemans and Bronner-Fraser, 2004; Monsoro-Burq et al., 2005; Nichane et al., 2008). In this early NC role, *Pax3* expression actually precedes *Sox10*. Our application of *Sox10*-cre was designed to interrogate later functions of *Pax3* based on the initial observation of strong *Pax3* expression in pelvic ganglia. We were fortunate that the activation of *Sox10*-cre, subsequent excision of $Pax3^{flox}$ allele, and decay of original Pax3 protein from the floxed locus provided sufficient delay that these mice survived postnatally as early loss of *Pax3* leads to cardiac defects that are lethal (Conway et al., 1997). While it might have been possible to incorporate a cre driver regulated by an early NC gene such as *Tfap2a*, this would likely lead to fetal lethality and prevented the analysis of bladder innervation we aimed to achieve. The $Pax3^{Sp\text{-}d/\Delta 5}$ mice we describe do not exhibit neural tube defects; however, they offer a novel model for understanding the sources of pediatric bladder dysfunction.

The *Sox10*-H2BVenus transgene strategy we applied facilitates tracing of migratory NC as they colonize the bladder body. This approach is advantageous as a nuclear label that distinguishes individual cells, is a single allele system that simplifies crosses compared to multi-allelic cre:LoxP strategies, and illuminates active expression of *Sox10* in NCPs in the periphery. Importantly, use of *Sox10*-H2BVenus allowed us to discriminate between NCPs and differentiating neurons that down-regulate the transgene and begin to express HuC/D. In

our analysis, Ki67 labeling identified active cell proliferation among both Venus+ NCPs and HuC/D+ neurons within pelvic ganglia. Proliferation of neuronal progenitors in the murine CNS is widely known, although fewer reports exist for active proliferation of committed neuronal progenitors in the peripheral nervous system. Use of the *Sox10*-H2BVenus allowed us to recognize that this process was distinct from NCP proliferation that we might have missed if we had relied on Cre:LoxP labeling alone.

While the studies presented provide greater insight into the role of *Pax3* in pelvic ganglia neurogenesis, additional questions remain. It has previously been shown that reduced expression of *Pax3* inhibits sensory neuron development *in vitro* (Koblar et al., 1999). Thus, some aspects of the altered voiding behavior observed in $Pax3^{Sp\text{-}d/\Delta 5}$ mutant mice could be attributable to altered bladder sensory innervation. Because developing sensory neurons and developing pelvic ganglia neurons both express CGRP, it is challenging to discern the effect of Pax3 on bladder sensory innervation in fetal stages. Investigation of sensory versus motor effects in these mice must await dorsal root versus pelvic autonomic neuron specific gene deletion in the future. $Pax3^{Sp\text{-}d/\Delta 5}$ mice were capable of voiding and we detected changes in their VSA patterns relative to wild type littermates indicating altered bladder function. While we did not observe overt bladder enlargement or hypertrophy in these mice at the time of tissue harvest between 5-6 weeks of age, it is possible that these mutants experience urinary retention, a common bladder problem among SB patients. VSA does not provide information on detrusor contractility or urinary retention, unless it is dramatic. Future analysis of bladder contractility and other physiological phenotypes in $Pax3^{Sp\text{-}d/\Delta 5}$ mice could be undertaken using cystometry or a newly modified uroflowmetry method that enables real time monitoring of voiding (Wang et al., 2019) that may detect more subtle phenotypes than we observed with VSA studies. Male SB patients suffer from sexual dysfunction (Deng et al., 2018; Roth et al., 2021). We did not maintain $Pax3^{Sp\text{-}d/\Delta 5}$ mice beyond 6 weeks of age or attempt to breed them because they were already smaller than littermates and their malocclusion would have required regular trimming of their teeth. Whether these mice are fertile and capable of breeding is open to investigation and may provide greater insight into the mechanisms of sexual dysfunction in male SB patients. Lastly, we did not assess changes in the bladder wall of aged $Pax3^{Sp\text{-}d/\Delta 5}$ mice due to the challenges that their maintenance would require. Neurogenic bladder in SB patients leads to progressive morphological changes in the bladder wall over time. Whether these mutants develop bladder wall fibrosis as they age remains open to future study. Altogether, these aspects emphasize the need to continue pursuit of animal models of SB and the $Pax3^{Sp\text{-}d/\Delta 5}$ model is one of very few viable models that will enable such analysis.

In this study, we demonstrate that the pelvic ganglia of *Pax3* variants exhibit delayed neurogenesis in fetal stages and that NC-specific deletion of *Pax3* leads to altered innervation in bladders of post-natal mice. Collectively, these results identify a novel role for *Pax3* in bladder innervation, demonstrate that *Pax3* expression within neural crest is required for normal bladder innervation, and provide evidence that alterations in development of pelvic ganglia can lead to bladder dysfunction.

Acknowledgements

We thank Dr. Vanda Lennon for generously providing HuC/D antibody. We greatly appreciate the technical assistance of Ms. Marisa Rigsby, particularly with respect to mouse husbandry, dissections, and gel imaging. We gratefully acknowledge the staff of the Cell Imaging Shared Resource Core at Vanderbilt University for advice and assistance in confocal imaging. The Cell Imaging Shared Resource Core is supported by NIH grants CA68485, DK20593, P30DK058404, DK59637 and EY08126. This work was supported by funding from US National Institutes of Health grants from NIDDK (R01-DK078158; U01-DK110804) to E.M.S^{2}. MMB was supported by a Vanderbilt SURP Scholarship. ASC was supported by a Cornelius Vanderbilt Scholarship for summer research.

References

Anderson RB, Stewart AL, Young HM, 2006. Phenotypes of neural-crest-derived cells in vagal and sacral pathways. Cell Tissue Res 323, 11–25. [PubMed: 16133146]

Arellano J, Xelhuantzi N, Mirto N, Hernandez ME, Cruz Y, 2019. Neural interrelationships of autonomic ganglia from the pelvic region of male rats. Auton Neurosci 217, 26–34. [PubMed: 30704972]

Barber TD, Barber MC, Tomescu O, Barr FG, Ruben S, Friedman TB, 2002. Identification of target genes regulated by PAX3 and PAX3-FKHR in embryogenesis and alveolar rhabdomyosarcoma. Genomics 79, 278–284. [PubMed: 11863357]

Bjorling DE, Wang Z, Vezina CM, Ricke WA, Keil KP, Yu W, Guo L, Zeidel ML, Hill WG, 2015. Evaluation of voiding assays in mice: impact of genetic strains and sex. Am J Physiol Renal Physiol 308, F1369–1378. [PubMed: 25904700]

Borycki AG, Li J, Jin F, Emerson CP, Epstein JA, 1999. Pax3 functions in cell survival and in pax7 regulation. Development 126, 1665–1674. [PubMed: 10079229]

Bult CJ, Blake JA, Smith CL, Kadin JA, Richardson JE, Mouse Genome Database, G., 2019. Mouse Genome Database (MGD) 2019. Nucleic Acids Res 47, D801–D806. [PubMed: 30407599]

Cass AS, Spence BR, 1973. Urinary incontinence in myelomeningocele. J Urol 110, 136–137. [PubMed: 4576595]

Conway SJ, Henderson DJ, Copp AJ, 1997. Pax3 is required for cardiac neural crest migration in the mouse: evidence from the splotch (Sp2H) mutant. Development 124, 505–514. [PubMed: 9053326]

Copp AJ, Adzick NS, Chitty LS, Fletcher JM, Holmbeck GN, Shaw GM, 2015. Spina bifida. Nat Rev Dis Primers 1, 15007. [PubMed: 27189655]

Deal KK, Rosebrock JC, Eeds AM, DeKeyser JL, Musser MA, Ireland SJ, May-Zhang AA, Buehler DP, Southard-Smith EM, 2020. Sox10-cre BAC transgenes reveal temporal restriction of mesenchymal cranial neural crest and identify glandular Sox10 expression. Dev Biol.

Deng N, Thirumavalavan N, Beilan JA, Tatem AJ, Hockenberry MS, Pastuszak AW, Lipshultz LI, 2018. Sexual dysfunction and infertility in the male spina bifida patient. Transl Androl Urol 7, 941–949. [PubMed: 30505732]

Dickie MM, 1964. New Splotch Alleles in the Mouse. J Hered 55, 97–101. [PubMed: 14170406]

Doddrell RD, Dun XP, Moate RM, Jessen KR, Mirsky R, Parkinson DB, 2012. Regulation of Schwann cell differentiation and proliferation by the Pax-3 transcription factor. Glia 60, 1269–1278. [PubMed: 22532290]

Dude CM, Kuan CY, Bradshaw JR, Greene ND, Relaix F, Stark MR, Baker CV, 2009. Activation of Pax3 target genes is necessary but not sufficient for neurogenesis in the ophthalmic trigeminal placode. Dev Biol 326, 314–326. [PubMed: 19100251]

Dyachuk V, Furlan A, Shahidi MK, Giovenco M, Kaukua N, Konstantinidou C, Pachnis V, Memic F, Marklund U, Muller T, Birchmeier C, Fried K, Ernfors P, Adameyko I, 2014. Neurodevelopment. Parasympathetic neurons originate from nerve-associated peripheral glial progenitors. Science 345, 82–87. [PubMed: 24925909]

Engleka KA, Gitler AD, Zhang M, Zhou DD, High FA, Epstein JA, 2005. Insertion of Cre into the Pax3 locus creates a new allele of Splotch and identifies unexpected Pax3 derivatives. Dev Biol 280, 396–406. [PubMed: 15882581]

Espinosa-Medina I, Outin E, Picard CA, Chettouh Z, Dymecki S, Consalez GG, Coppola E, Brunet JF, 2014. Neurodevelopment. Parasympathetic ganglia derive from Schwann cell precursors. Science 345, 87–90. [PubMed: 24925912]

Goulding MD, Chalepakis G, Deutsch U, Erselius JR, Gruss P, 1991. Pax-3, a novel murine DNA binding protein expressed during early neurogenesis. EMBO J 10, 1135–1147. [PubMed: 2022185]

Harris MJ, Juriloff DM, 2010. An update to the list of mouse mutants with neural tube closure defects and advances toward a complete genetic perspective of neural tube closure. Birth Defects Res A Clin Mol Teratol 88, 653–669. [PubMed: 20740593]

Hauswirth R, Haase B, Blatter M, Brooks SA, Burger D, Drogemuller C, Gerber V, Henke D, Janda J, Jude R, Magdesian KG, Matthews JM, Poncet PA, Svansson V, Tozaki T, Wilkinson-White L, Penedo MCT, Rieder S, Leeb T, 2019. Correction: Mutations in MITF and PAX3 Cause "Splashed White" and Other White Spotting Phenotypes in Horses. PLoS Genet 15, e1008321. [PubMed: 31374075]

Hol FA, Hamel BC, Geurds MP, Mullaart RA, Barr FG, Macina RA, Mariman EC, 1995. A frameshift mutation in the gene for PAX3 in a girl with spina bifida and mild signs of Waardenburg syndrome. J Med Genet 32, 52–56. [PubMed: 7897628]

Hornyak TJ, Hayes DJ, Chiu LY, Ziff EB, 2001. Transcription factors in melanocyte development: distinct roles for Pax-3 and Mitf. Mech Dev 101, 47–59. [PubMed: 11231058]

Kaufman MH, 1995. The Atlas of Mouse Development. Academic Press, San Diego.

Keil KP, Abler LL, Altmann HM, Bushman W, Marker PC, Li L, Ricke WA, Bjorling DE, Vezina CM, 2016. Influence of animal husbandry practices on void spot assay outcomes in C57BL/6J male mice. Neurourol Urodyn 35, 192–198. [PubMed: 25394276]

Koblar SA, Murphy M, Barrett GL, Underhill A, Gros P, Bartlett PF, 1999. Pax-3 regulates neurogenesis in neural crest-derived precursor cells. J Neurosci Res 56, 518–530. [PubMed: 10369218]

Koushik SV, Chen H, Wang J, Conway SJ, 2002. Generation of a conditional loxP allele of the Pax3 transcription factor that enables selective deletion of the homeodomain. Genesis 32, 114–117. [PubMed: 11857794]

Kubic JD, Young KP, Plummer RS, Ludvik AE, Lang D, 2008. Pigmentation PAX-ways: the role of Pax3 in melanogenesis, melanocyte stem cell maintenance, and disease. Pigment Cell Melanoma Res 21, 627–645. [PubMed: 18983540]

Li X, James WM, Traganos F, Darzynkiewicz Z, 1995. Application of biotin, digoxigenin or fluorescein conjugated deoxynucleotides to label DNA strand breaks for analysis of cell proliferation and apoptosis using flow cytometry. Biotech Histochem 70, 234–242. [PubMed: 8580207]

Lin J, Fu S, Yang C, Redies C, 2017. Pax3 overexpression induces cell aggregation and perturbs commissural axon projection during embryonic spinal cord development. J Comp Neurol 525, 1618–1632. [PubMed: 27864937]

Lin J, Wang C, Yang C, Fu S, Redies C, 2016. Pax3 and Pax7 interact reciprocally and regulate the expression of cadherin-7 through inducing neuron differentiation in the developing chicken spinal cord. J Comp Neurol 524, 940–962. [PubMed: 26287727]

Lu W, Zhu H, Wen S, Laurent C, Shaw GM, Lammer EJ, Finnell RH, 2007. Screening for novel PAX3 polymorphisms and risks of spina bifida. Birth Defects Res A Clin Mol Teratol 79, 45–49. [PubMed: 17149730]

Madisen L, Zwingman TA, Sunkin SM, Oh SW, Zariwala HA, Gu H, Ng LL, Palmiter RD, Hawrylycz MJ, Jones AR, Lein ES, Zeng H, 2010. A robust and high-throughput Cre reporting and characterization system for the whole mouse brain. Nat Neurosci 13, 133–140. [PubMed: 20023653]

Meulemans D, Bronner-Fraser M, 2004. Gene-regulatory interactions in neural crest evolution and development. Dev Cell 7, 291–299. [PubMed: 15363405]

Milet C, Maczkowiak F, Roche DD, Monsoro-Burq AH, 2013. Pax3 and Zic1 drive induction and differentiation of multipotent, migratory, and functional neural crest in Xenopus embryos. Proc Natl Acad Sci U S A 110, 5528–5533. [PubMed: 23509273]

Minchin JE, Hughes SM, 2008. Sequential actions of Pax3 and Pax7 drive xanthophore development in zebrafish neural crest. Dev Biol 317, 508–522. [PubMed: 18417109]

Mohd-Zin SW, Marwan AI, Abou Chaar MK, Ahmad-Annuar A, Abdul-Aziz NM, 2017. Spina Bifida: Pathogenesis, Mechanisms, and Genes in Mice and Humans. Scientifica (Cairo) 2017, 5364827. [PubMed: 28286691]

Monsoro-Burq AH, 2015. PAX transcription factors in neural crest development. Semin Cell Dev Biol 44, 87–96. [PubMed: 26410165]

Monsoro-Burq AH, Wang E, Harland R, 2005. Msx1 and Pax3 cooperate to mediate FGF8 and WNT signals during Xenopus neural crest induction. Dev Cell 8, 167–178. [PubMed: 15691759]

Mundell NA, Plank JL, LeGrone AW, Frist AY, Zhu L, Shin MK, Southard-Smith EM, Labosky PA, 2012. Enteric nervous system specific deletion of Foxd3 disrupts glial cell differentiation and activates compensatory enteric progenitors. Dev Biol 363, 373–387. [PubMed: 22266424]

Nakazaki H, Reddy AC, Mania-Farnell BL, Shen YW, Ichi S, McCabe C, George D, McLone DG, Tomita T, Mayanil CS, 2008. Key basic helix-loop-helix transcription factor genes Hes1 and Ngn2 are regulated by Pax3 during mouse embryonic development. Dev Biol 316, 510–523. [PubMed: 18308300]

Nichane M, de Croze N, Ren X, Souopgui J, Monsoro-Burq AH, Bellefroid EJ, 2008. Hairy2-Id3 interactions play an essential role in Xenopus neural crest progenitor specification. Dev Biol 322, 355–367. [PubMed: 18721802]

Olaopa M, Zhou HM, Snider P, Wang J, Schwartz RJ, Moon AM, Conway SJ, 2011. Pax3 is essential for normal cardiac neural crest morphogenesis but is not required during migration nor outflow tract septation. Dev Biol 356, 308–322. [PubMed: 21600894]

Rajandram R, Ong TA, Razack AH, MacIver B, Zeidel M, Yu W, 2016. Intact urothelial barrier function in a mouse model of ketamine-induced voiding dysfunction. Am J Physiol Renal Physiol 310, F885–894. [PubMed: 26911853]

Ritter KE, Wang Z, Vezina CM, Bjorling DE, Southard-Smith EM, 2017. Serotonin Receptor 5-HT3A Affects Development of Bladder Innervation and Urinary Bladder Function. Front Neurosci 11, 690. [PubMed: 29311772]

Roth JD, Spinoit AF, Hoebeke P, 2021. Sexual function and dysfunction in men with spina bifida. J Pediatr Urol.

Shapiro E, Seller MJ, Lepor H, Kalousek DK, Hutchins GM, Perlman EJ, Meuli M, 1998. Altered smooth muscle development and innervation in the lower genitourinary and gastrointestinal tract of the male human fetus with myelomeningocele. J Urol 160, 1047–1053; discussion 1079. [PubMed: 9719274]

Shinoshima H, 2004. [Embryogenesis of bladder smooth muscle in delayed Splotch mice]. Hokkaido Igaku Zasshi 79, 389–397. [PubMed: 15373211]

Smith-Anttila CJ, Morrison V, Keast JR, 2021. Spatiotemporal mapping of sensory and motor innervation of the embryonic and postnatal mouse urinary bladder. Dev Biol.

Snow-Lisy DC, Yerkes EB, Cheng EY, 2015. Update on Urological Management of Spina Bifida from Prenatal Diagnosis to Adulthood. J Urol 194, 288–296. [PubMed: 25839383]

Southard-Smith EM, 2012. GUDMAP Consortium, https://www.gudmap.org/id/N-GWRP.

Underhill DA, Vogan KJ, Gros P, 1995. Analysis of the mouse Splotch-delayed mutation indicates that the Pax-3 paired domain can influence homeodomain DNA-binding activity. Proc Natl Acad Sci U S A 92, 3692–3696. [PubMed: 7731966]

Wang X, Chan AK, Sham MH, Burns AJ, Chan WY, 2011. Analysis of the sacral neural crest cell contribution to the hindgut enteric nervous system in the mouse embryo. Gastroenterology 141, 992–1002 e1001-1006. [PubMed: 21699792]

Wang Z, Guzman EC, Nimunkar A, Keil KP, Vezina CM, Ricke WA, Macoska J, Bjorling DE, 2019. Void sorcerer: an open source, open access framework for mouse uroflowmetry. Am J Clin Exp Urol 7, 170–177. [PubMed: 31317056]

Wanigasekara Y, Kepper ME, Keast JR, 2003. Immunohistochemical characterisation of pelvic autonomic ganglia in male mice. Cell Tissue Res 311, 175–185. [PubMed: 12596037]

Wiener JS, Suson KD, Castillo J, Routh JC, Tanaka ST, Liu T, Ward EA, Thibadeau JK, Joseph DB, National Spina Bifida Patient, R., 2018. Bladder Management and Continence Outcomes in Adults

with Spina Bifida: Results from the National Spina Bifida Patient Registry, 2009 to 2015. J Urol 200, 187–194. [PubMed: 29588216]

Wiese CB, Deal KK, Ireland SJ, Cantrell VA, Southard-Smith EM, 2017. Migration pathways of sacral neural crest during development of lower urogenital tract innervation. Dev Biol 429, 356–369. [PubMed: 28449850]

Wiese CB, Ireland S, Fleming NL, Yu J, Valerius MT, Georgas K, Chiu HS, Brennan J, Armstrong J, Little MH, McMahon AP, Southard-Smith EM, 2012. A genome-wide screen to identify transcription factors expressed in pelvic Ganglia of the lower urinary tract. Front Neurosci 6, 130. [PubMed: 22988430]

Yu W, Ackert-Bicknell C, Larigakis JD, MacIver B, Steers WD, Churchill GA, Hill WG, Zeidel ML, 2014. Spontaneous voiding by mice reveals strain-specific lower urinary tract function to be a quantitative genetic trait. Am J Physiol Renal Physiol 306, F1296–1307. [PubMed: 24717733]

Zhou HM, Wang J, Rogers R, Conway SJ, 2008. Lineage-specific responses to reduced embryonic Pax3 expression levels. Dev Biol 315, 369–382. [PubMed: 18243171]

Highlights:

- *Pax3*$^{Sp\text{-}d}$ sacral NC exhibit deficient migration during colonization of bladder.
- Proliferation of progenitors within pelvic ganglia is altered in *Pax3*$^{Sp\text{-}d}$ mutants.
- *Pax3*$^{Sp\text{-}d}$ mutants exhibit aberrant pelvic ganglia neurogenesis.
- NC-specific deletion of *Pax3* alters density and patterning of bladder innervation.
- NC-specific *Pax3*$^{Sp\text{-}d/\Delta 5}$ mutants are viable with altered bladder innervation and urination patterns

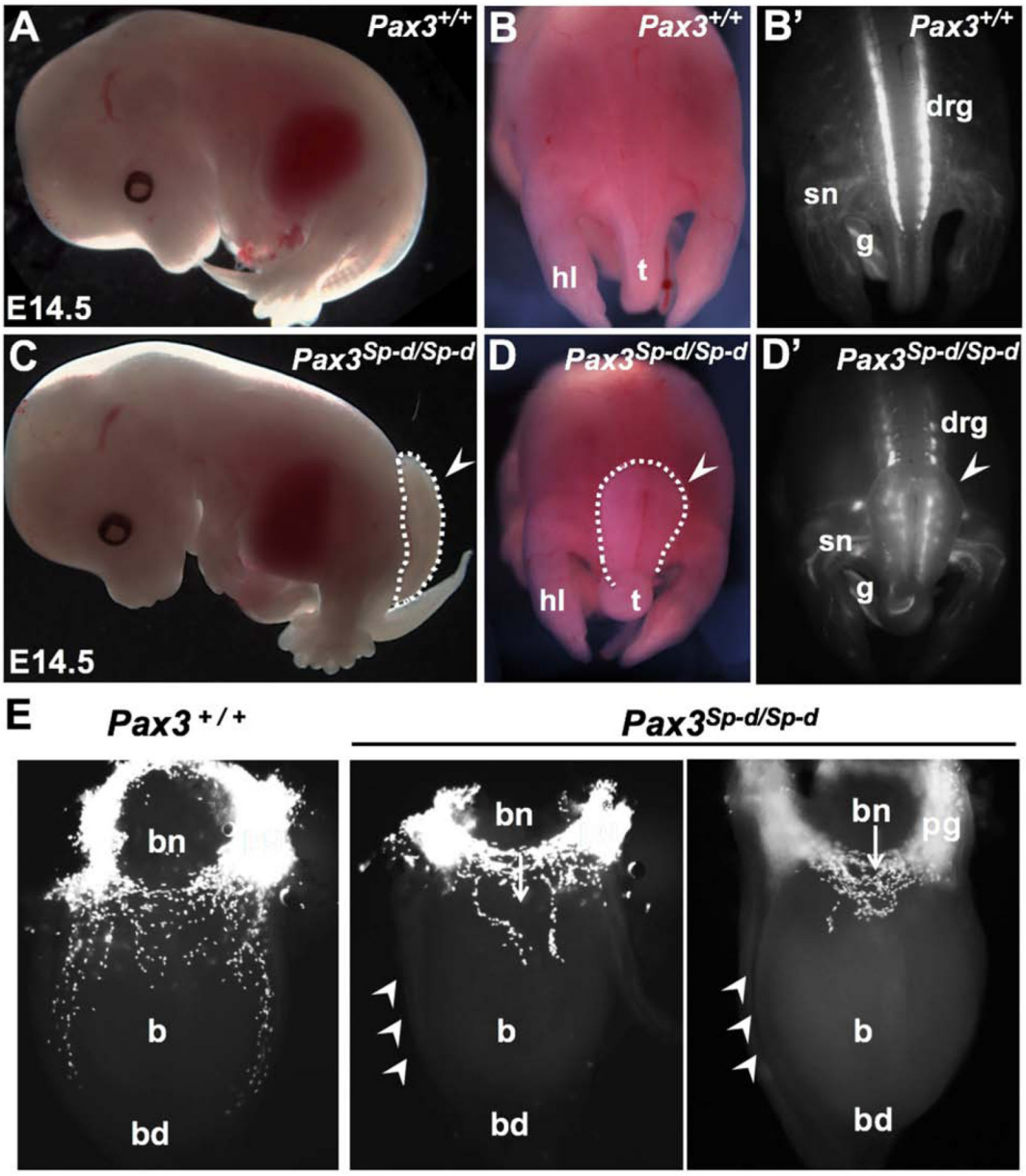

Figure 1. Altered neural crest development revealed by *Sox10*-H2BVenus transgene expression in *Pax3*$^{Sp\text{-}d/Sp\text{-}d}$ embryos.

Whole mount lateral views of *Pax3*$^{+/+}$;*Sox10*-H2BVenus (**A**) and homozygous *Pax3*$^{Sp\text{-}d/Sp\text{-}d}$;*Sox10*-H2BVenus (**C**) littermates show caudal rachischisis (arrowheads/dashed area) in mutants at 14.5 dpc. Dorsal bright field and fluorescence images of fetal spine of WT embryos (**B,B'**) and *Pax3*$^{Sp\text{-}d/Sp\text{-}d}$ mutants (**D,D'**) show open neural tube, bent tail, and misshapen sacral DRG revealed by *Sox10*-H2BVenus transgene labeling. Ventral views (**E**) of micro-dissected bladder from wild type *Pax3*$^{+/+}$ relative to *Pax3*$^{Sp\text{-}d/Sp\text{-}d}$ shows aberrant migration of Sox10+ NCPs in lateral streams (arrowheads) and medial populations (arrows). Abbreviations: **b**, bladder; **bd**, bladder dome; **bn**, bladder neck; **drg**, dorsal root ganglia; **g**, gut; **hl**, hindlimb; **pg**, pelvic ganglia; **sn**, sciatic nerve; **t**, tail.

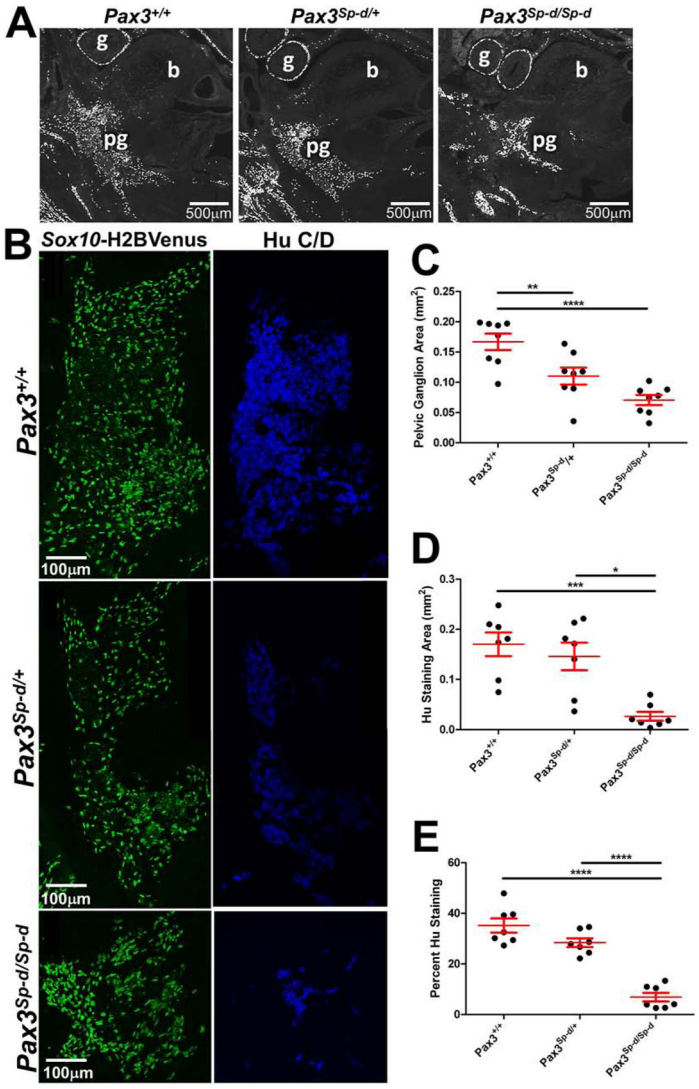

Figure 2. *Pax3*$^{Sp\text{-}d/Sp\text{-}d}$ pelvic ganglia exhibit reduced neuronal commitment in midgestation.

(**A**) Fluorescent images of parasagittal sections from 14.5 dpc embryos obtained at comparable anatomic levels are shown. *Sox10* transgene fluorescence illuminates PG, enteric nervous system in the fetal gut, and peripheral nerve fibers. (**B**) Higher magnification images of *Sox10*-H2BVenus transgene fluorescence (left) in cryosections from each of the *Pax3* genotypes immunostained for HuC/D (blue, right). (**C**) Plot of pelvic ganglia area, as delineated by *Sox10*-H2BVenus expression. (**D**) Plot of pelvic ganglia area stained by HuC/D. (**E**) Plot of percent HuC/D area relative to total PG area. Each dot in plots **C-E** represents the average value for an independent embryo from which 5-6 PG sections were imaged (n=7-8 distinct embryos per genotype class). Average ± SEM (red lines). Statistical significance was determined by Tukey's HSD between genotypes: * $p<0.05$; ** $p<0.01$; *** $p<0.001$; **** $p<0.0001$. Abbreviations: **b**, bladder; **g**, gut; **pg**, pelvic ganglia.

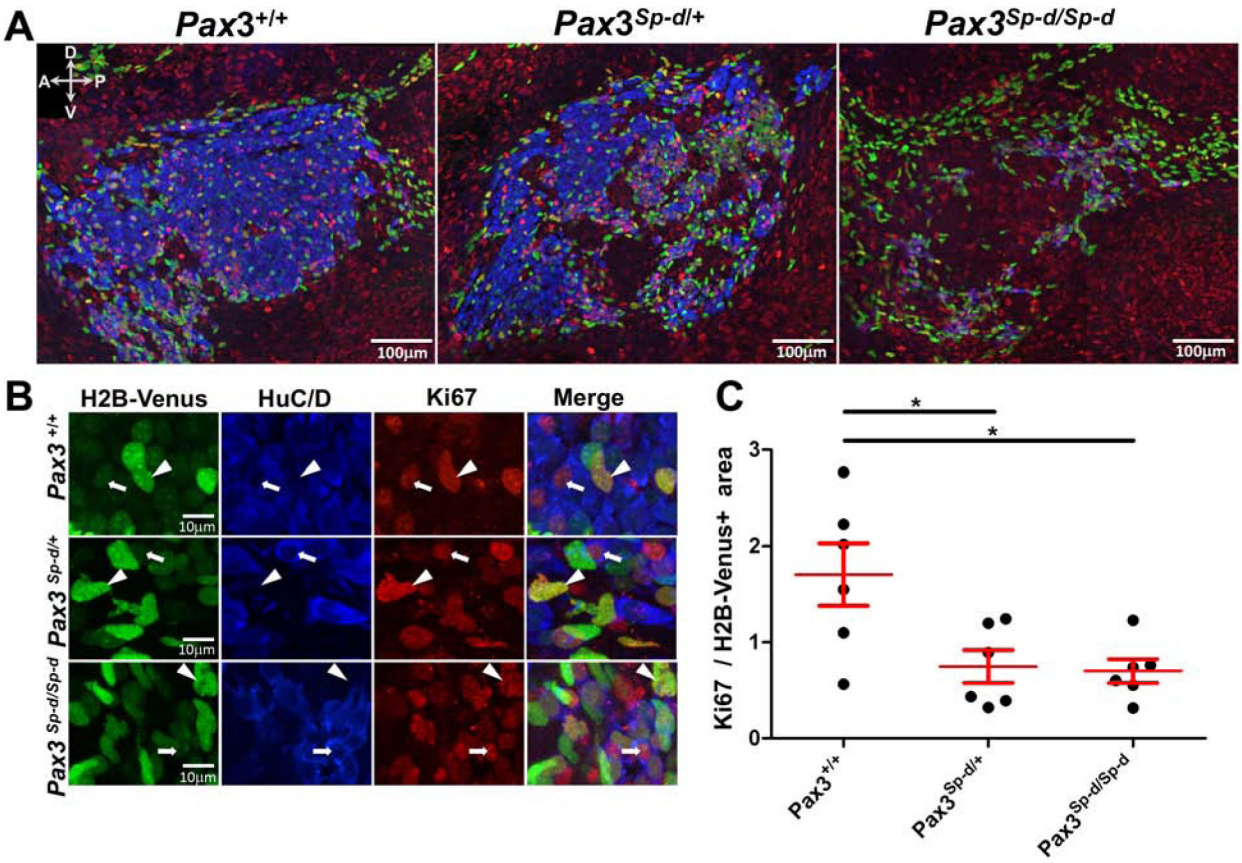

Figure 3. Proliferation of Sox10+ progenitors and differentiating neurons within pelvic ganglia is reduced in *Pax3*$^{Sp\text{-}d/Sp\text{-}d}$ embryos.

(**A**) Confocal images of Sox10-H2BVenus transgene expression (green) in cryosections of 14.5 dpc PG stained with HuC/D (blue) and Ki67 (red) to detect proliferating cells. (**B**) High magnification confocal images (630X) from each genotype show co-localization of H2B-Venus+ signal with Ki67+ (arrowheads) as well as of Ki67+ HuC/D+ differentiating neurons (arrows). (**C**) Plot of percent Ki67 over total area of pelvic ganglia defined by area of H2BVenus expression. Proliferation detected by Ki67 immunolabeling is significantly reduced proliferation within pelvic ganglia between *Pax3*$^{+/+}$ and *Pax3*$^{Sp\text{-}d/Sp\text{-}d}$ embryos ($p \leq 0.05$) and *Pax3*$^{+/+}$ and *Pax3*$^{Sp\text{-}d/+}$ embryos ($p \leq 0.05$). Each dot represents values for an independent embryo averaged across measures from three pelvic ganglia sections. Average ± SEM (red lines). * $p < 0.05$

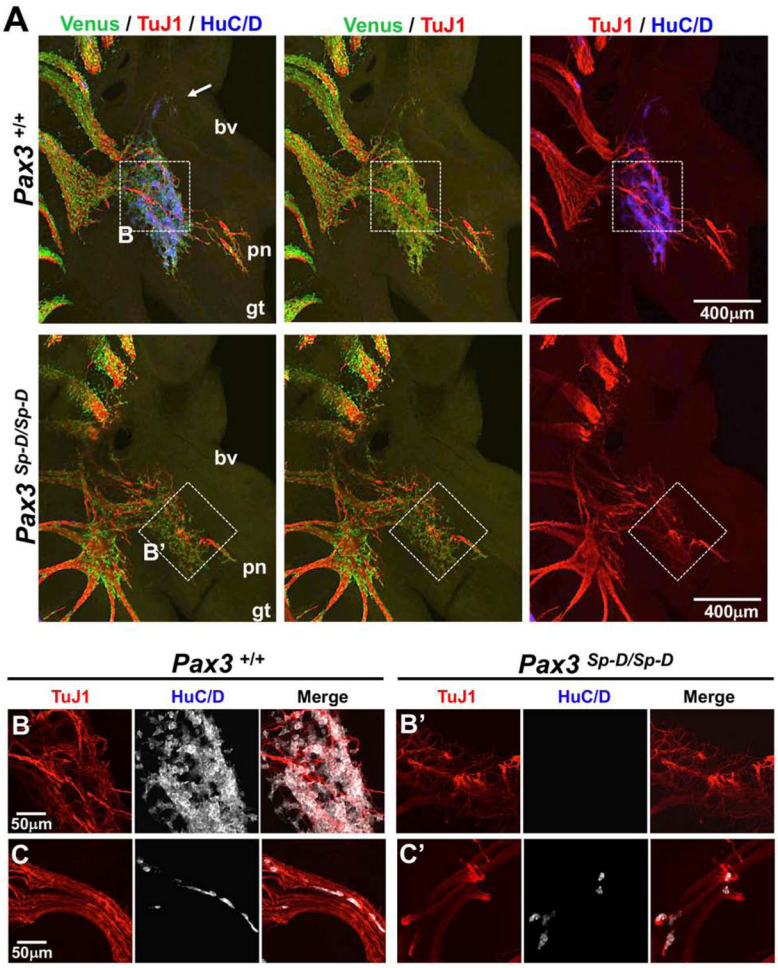

Figure 4. Sox10+ NPCs migrate appropriately into the developing urogenital system of *Pax3*$^{Sp\text{-}d/Sp\text{-}d}$ mutants but fail to initiate neurogenesis by 12.5 dpc.

(A) Tiled confocal images of vibratome sections through sacral regions of *Pax3*$^{+/+}$ (upper panels) and *Pax3*$^{Sp\text{-}d/Sp\text{-}d}$ (lower panels) embryos expressing *Sox10*-H2BVenus transgene expression (green) at 12.5 dpc. TuJ1 (red) labeling that detects nerve fiber processes entering the lower urinary tract is similar between genotypes. Immunolabeling for HuC/D (blue) that detects differentiating neurons is absent from the region where NPCs aggregate at the base of the genital tubercle in *Pax3*$^{Sp\text{-}d/Sp\text{-}d}$ embryos. (**B, B'**) High magnification images of boxed regions in A panels shows absence of HuC/D labeling despite the presence of TuJ1 positive nerve fibers. (**C, C'**) High magnification images of nerve bundles coming from dorsal root ganglion (out of the field of view in A, A' panels) show migration of HuC/D positive progenitors along TuJ1 positive nerve fibers in both *Pax3*$^{+/+}$ and *Pax3*$^{Sp\text{-}d/Sp\text{-}d}$ embryos. Abbreviations: **bv**, blood vessel; **gt**, genital tubercle; **pn**, pudendal nerve.

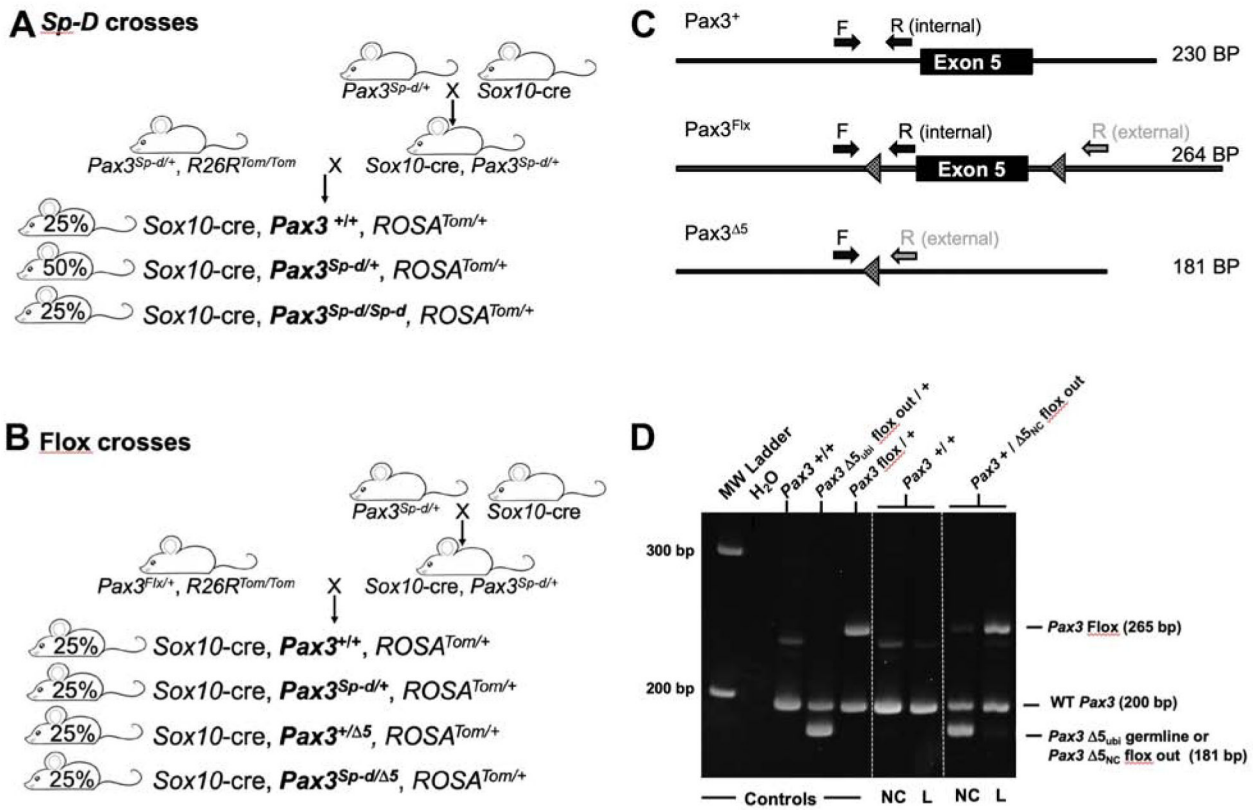

Figure 5. Crosses and genotyping assays to derive NC-specific deletion of *Pax3* for comparison with *Pax3*$^{Sp-d}$ mutants.

(**A**) Schematic diagram of crosses performed to enable NC lineage tracing in *Pax3*$^{Sp-d}$ offspring using the *Sox10*-cre line in combination with *ROSA*^{Tom} reporter. (**B**) Schematic of crosses performed to enable NC-specific deletion of *Pax3*^{flox} allele in combination with the *Pax3*$^{Sp-d}$ allele. (**C**) Diagram of PCR oligonucleotide primer placement to detect wild type and *Pax3*^{flox} alleles. (**D**) Image of ethidium bromide stained-PCR products separated by gel electrophoresis for the various genotype possibilities illustrating appropriate excision of the *Pax3*^{flox} construct when crossed to the *Sox10*-cre line. PCR products are adjacent to a 100bp Molecular Weight ladder (far left), with four control DNA samples run left to right: Lane 1, H2O no template added; Lane 2, wild type C57BL/6J DNA; Lane 3, adult B6.Pax3$^{\Delta 5/+}$ DNA (exon 5 deleted in germline therefore ubiquitous deletion of flox cassette); Lane 4, adult B6. *Pax3*^{flox} with intact exon5 flanked by flox sites. The additional four lanes indicate the ability to concomitantly use the combination of predominantly NC-derived tissue from the fetal snout (NC) and non-NC-derived tissue from fetal liver (L) collected for each embryo to distinguish each of the four possible *Pax3* genotypic variants prior to immunohistochemical analysis of pelvic ganglia.

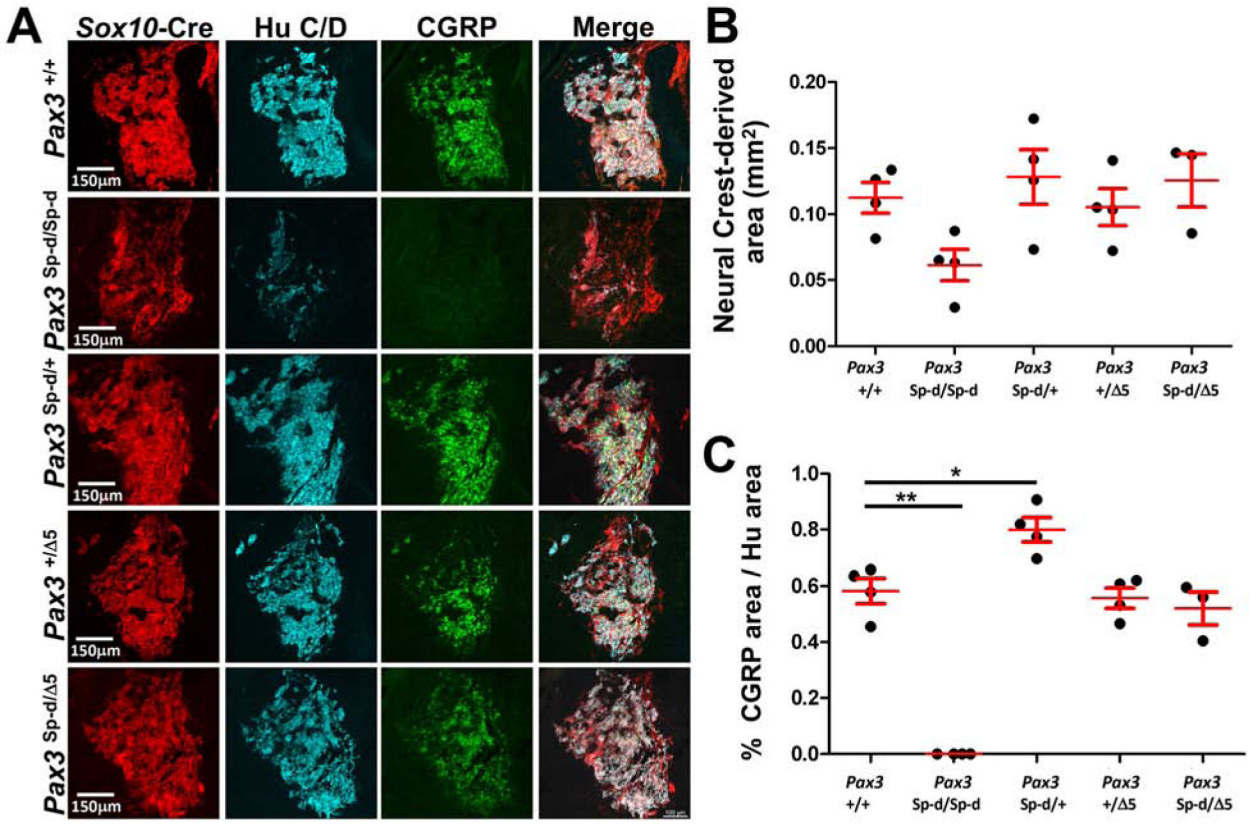

D

Genotype	Sample size	NCC Derivative Area (mm2) (average ± SEM)	*Hu*+ Area (mm2) (average ± SEM)	*CGRP*+ Area (mm2) (average ± SEM)	*CGRP/Hu* Ratio (average ± SEM)
+/+	n=4	0.113 ± 0.011	0.0451 ± 0.005	0.0265 0.004	0.582 ± 0.045
Sp-d/Sp-d	n=4	0.0614 ± 0.012	0.00569 ± 0.001	0 ± 0	**0 ± 0**
Sp-d/+	n=4	0.128± 0.021	0.00475 ± 0.016	0.0365 ± 0.012	**0.799 ± 0.044**
+/Δ5	n=4	0.106 ± 0.014	0.0431 ± 0.008	0.0238 ± 0.006	0.557 ± 0.036
Sp-d/Δ5	n=3	0.126 ± 0.020	0.0516 ± 0.010	0.0281 ± 0.008	0.520 ± 0.059

Figure 6. Constitutive *Pax3*^{Spd} mutant disrupts expression of CGRP in fetal pelvic ganglia while NC-specific *Pax3* ablation does not.

(**A**) Confocal Images of 14.5 dpc cryosections from *Pax3* variant genotypes stained for HuC/D and CGRP show total absence of CGRP expression in *Pax3*$^{Sp\text{-}d/Sp\text{-}d}$ PG. (**B**) Plot of total PG area of NC derivatives labeled by tdTomato activated via *Sox10*-cre for each genotype class. (**C**) Plot of percent CGRP labeling within total HuC/D area for each genotype class. Each dot represents average values for an independent embryo measured from six pelvic ganglia sections. Average ± SEM (red lines). * p<0.05; **p<0.01.

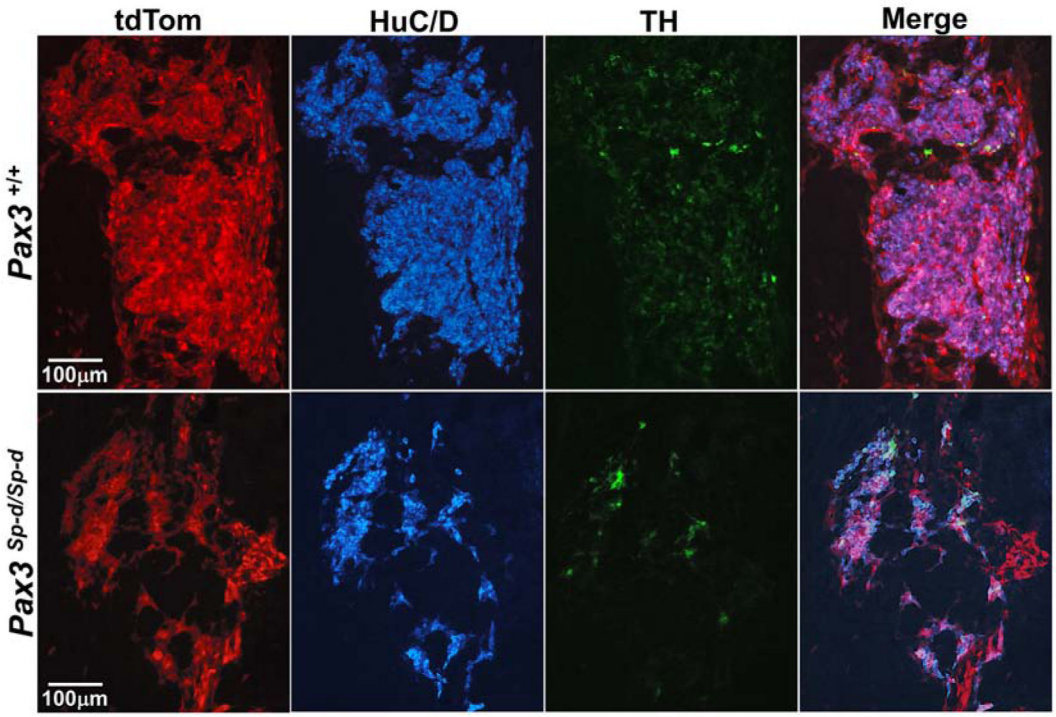

Figure 7. Constitutive *Pax3*^{Spd} mutation disrupts development of noradrenergic neurons in fetal pelvic ganglia.

Confocal images of cryosections through 14.5 dpc PG stained for noradrenergic neurons (TH+) relative to total HuC/D staining reveals that this neuron subtype is present although at reduced frequency in *Pax3*$^{Sp\text{-}d/Sp\text{-}d}$ mutant PG in contrast to the complete absence of CGRP + neurons.

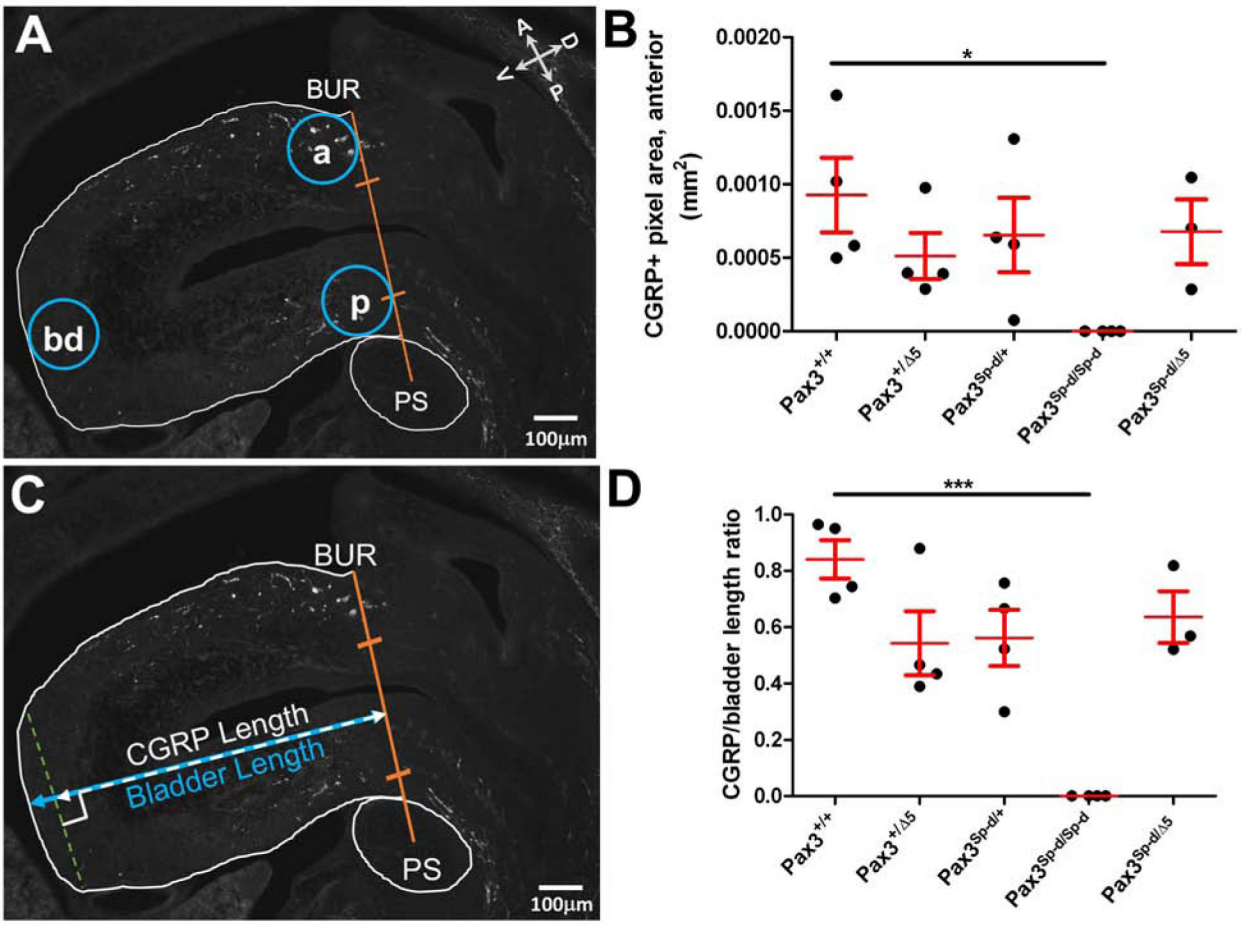

Figure 8. *Pax3* mutations in mice alter fetal bladder wall nerve fiber density and extent of innervation.

(**A**) Example image of nerve fiber quantitation in a sagittal cryosection through *Pax3*$^{+/+}$ 14.5 dpc bladder. Sections selected for presence of the bladder-ureteral reflection (BUR) and the pubic symphysis (PS) provided comparable anatomical planes. Pixel density in circular selections (blue) at anterior (a), posterior (p), and bladder dome (bd) were quantified. Directionality of anterior (A), dorsal (D), ventral (V), and posterior (P) are indicated. (**B**) Plot of CGRP+ nerve fiber density across genotype classes identifies significant difference for *Pax3*$^{Sp\text{-}d/Sp\text{-}d}$ mutants only in anterior regions. Each dot represents average values for independnt embryos (n=4) measured from five pelvic ganglia sections. Average ± SEM (red lines). *p<0.05. (**C**) Image illustrating measurement of the extent of bladder innervation as a function of overall bladder length. Perpendicular line drawn from the BUR-PS axis midpoint (orange line) to the bladder dome (blue line) defines bladder length compared to the furthest extent of CGRP+ fibers in the anterior bladder wall (white line). (**D**) Plot of CGRP+/bladder length ratio for all Pax3 genotype classes. Each dot represents one animal (n=3-4) measured from five sections. Average ± SEM (red lines). Significant differences in the CGRP/bladder length ratio were found between all genotypes when compared to *Pax3*$^{Sp\text{-}d/Sp\text{-}d}$ embryos; *p<0.05; ***p<0.001. Abbreviations: **BUR**, bladder-ureteral reflection; **PS**, pubic symphysis.

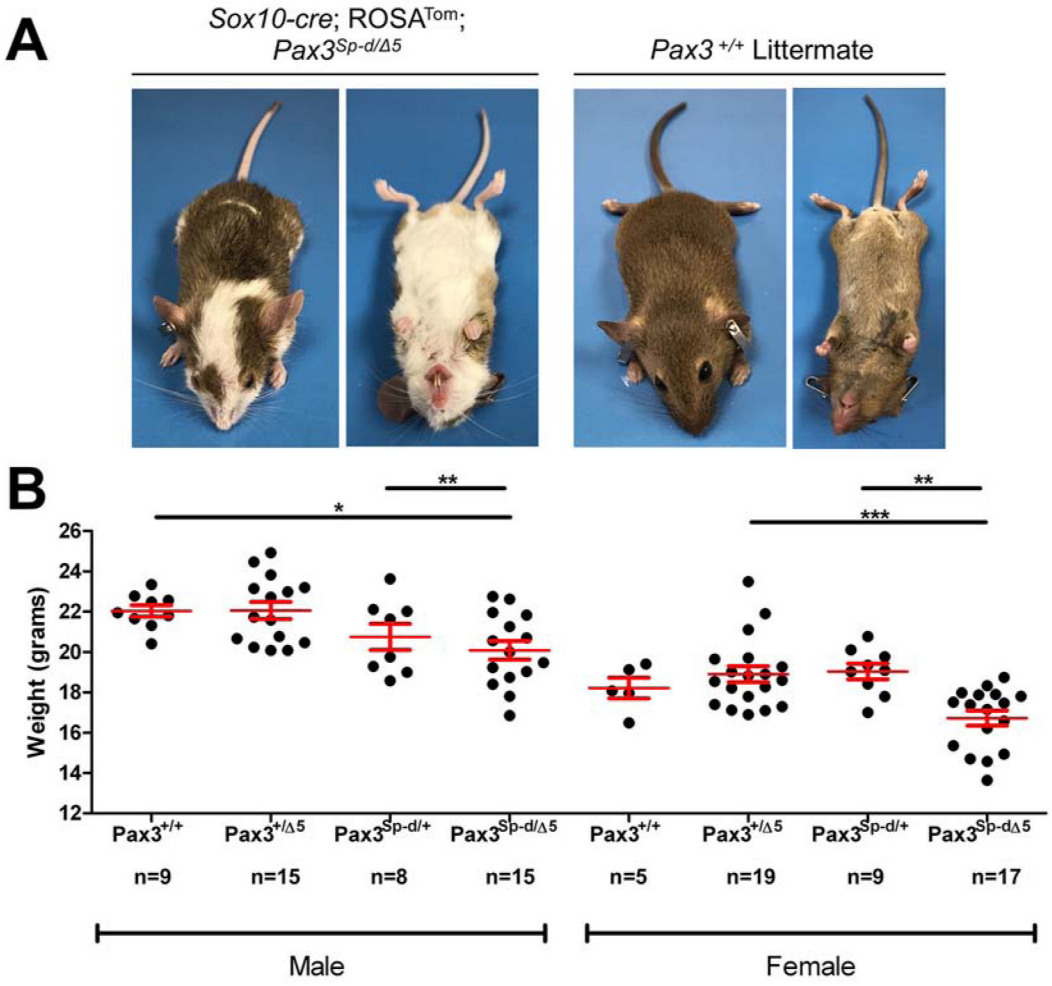

Figure 9. *Pax3*$^{Sp\text{-}d/\Delta 5}$ mice survive postnatally and exhibit NC phenotypes.

(**A**) *Pax3*$^{Sp\text{-}d/\Delta 5}$ mice show deficits in multiple NC-derived cell types including pigmentation deficits (melanocytes) and micrognathia with malocclusion (craniofacial). (**B**) Body weights of *Pax3* variant mice. *Pax3*$^{Sp\text{-}d/\Delta 5}$ mutants of both sexes weigh significantly less than littermates. * $p<0.05$; ** $p<0.01$; *** $p<0.001$.

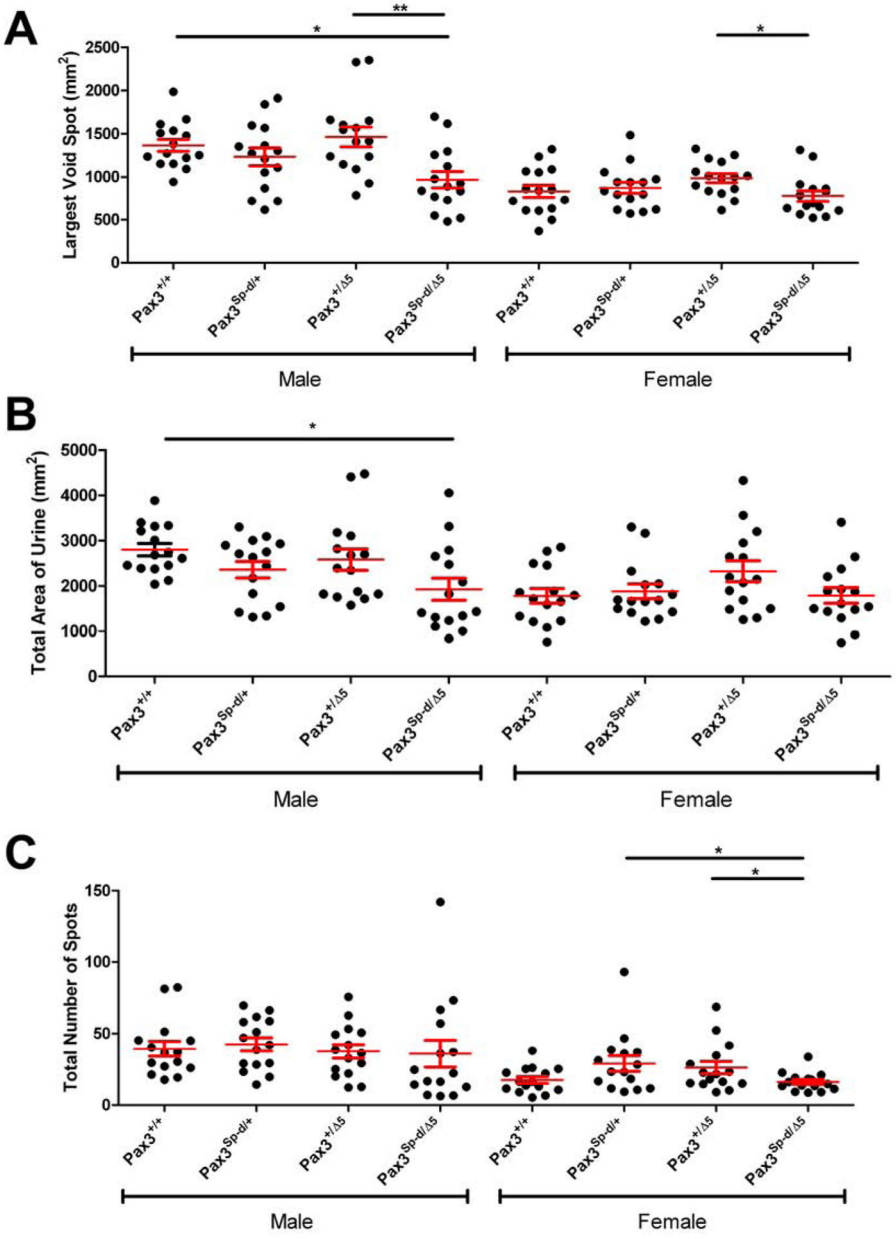

Figure 10. Urination patterns are altered in *Pax3*$^{Sp\text{-}d/\Delta5}$ male mice.

(**A**) Plot of average voiding frequency (number of individual voids over the testing period) assessed by VSA in male and female 4-week old mice. (**B**) Plot of average total area of all urine spots summed for the assay period. *Pax3*$^{Sp\text{-}d/\Delta5}$ males void significantly smaller area of urine than *Pax3*$^{+/+}$ littermates. (**C**) Plot of average largest void spot for all genotype classes. Primary void spots are significantly smaller for *Pax3*$^{Sp\text{-}d/\Delta5}$ males than *Pax3*$^{+/+}$ ($p \leq 0.005$). Black dots represent different individual animals within each genotype class. Average ± SEM (red lines). n=15 for all genotypes in each plot. *$p \leq 0.05$, ** $p \leq 0.01$

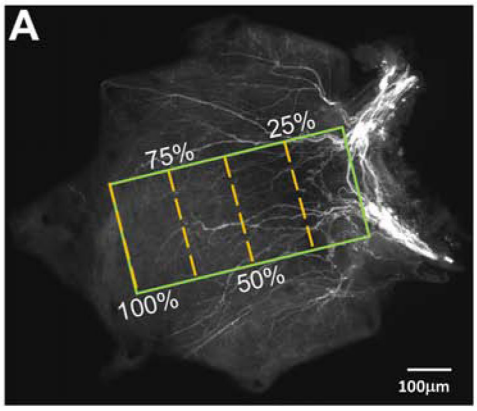

B

Male		Female	
Genotype	Percent Innervated	Genotype	Percent Innervated
+/+	7.62 ± 2.99	+/+	5.31 ± 2.07
+/Δ5	**3.59 ± 1.53**	+/Δ5	3.04 ± 1.88
Sp-d/+	**3.91 ± 1.73**	Sp-d/+	5.41 ± 2.66
Sp-d/Δ5	**3.42 ± 1.48**	Sp-d/Δ5	**1.85 ± 0.94**

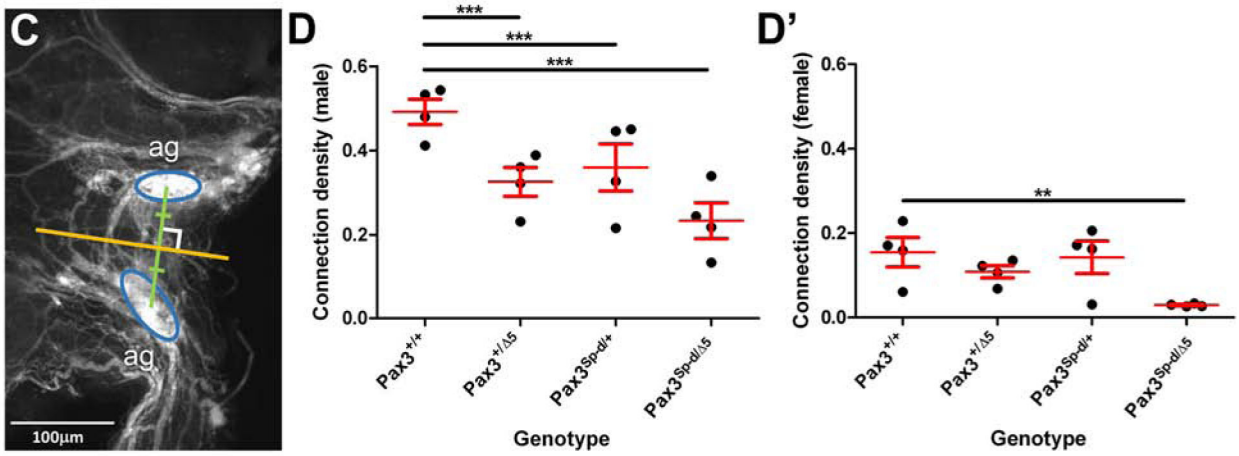

Figure 11. Alterations in *Pax3* affect interganglionic and bladder wall nerve fiber density in postnatal mice.

(**A**) Fluorescent whole mount image of *Sox10*-cre,ROSA^{Tom} bladder that relied on Tomato fluorescence to quantify neural projections. Pixel density was measured along a line (dotted orange) at 25, 50, 75, and 100% increments of a rectangle drawn to span the width between and extended towards the bladder dome. (**B**) Tabulated summary of bladder innervation density for *Pax3* variant genotype classes and sexes (n=4 per genotype per sex). Boldface percentages indicate values that differ significantly from wild type (p<0.05) based on a post-hoc test conducted with Tukey's HSD. (**C**) High magnification image of the bladder neck region used to assess interganglionic fiber density based on Tomato fluorescence. Segment drawn connecting the PG centers with a perpendicular line was placed at the midpoint, extending across the interganglionic fibers. Pixel density along perpendicular line (orange) was used to assess fiber density. (**D**, **D'**) Plots of fiber connection density for males and females (n=4 per class). Each dot represents a single animal. Average ± SEM (red lines). Post-hoc test conducted with Tukey's HSD (**, p<0.005, ***, p<0.0005). Abbreviations: **ag**, accessory ganglia.

Table 1.

Genotyping primers used for mouse lines in this study

Genotype	5’ to 3’ Sequence	PCR Parameters	Expected Product
Pax3^{WT} vs Pax3^{Spd}	**Forward:** CATTTCTCGCCAGCTTCGCGTG **WT Reverse:** AGGGCCGAGTCAACCAGCACG **Mutant Reverse:** AGTGTCCACCCCTCTTGGCCTCGGCCGAGTCAACCAGGTCC	94°C, 4 min; 30 cycles of: (94°C, 30 s; 63°C, 30 s; 0.5C/s to 74°C; 74°C, 30 s, ramp 0.5°C/s to 94°C); 74°C, 10 min	130bp **WT** 150bp **Spd** (Keller-Peck & Mullen, 1996),
Pax3^{Flx}	**Forward:** AAAGAAGTAGGCTGTTCATCG **Reverse:** AGTGAAGTTCAAAGTCGGAGTC	94°C, 5 min; 35 cycles of: (94°C, 30 s; 55°C, 30 s; ramp 0.5C/s to 72°C; 72°C, 30 s; ramp 0.5°C/s to 94°C); 72°C, 10 min	265bp
Pax 3^{WT} or Pax3^{Spd} vs Pax3$^{\Delta 5}$	**Forward:** GTTCAGCTTCAGGGTCTTTG **Internal Reverse:** TGAAGTTCAAAGTCGGAGTCT **External Reverse:** CTATGTCAACTAAGGGCTTTGG	92°C, 5 min; 36 cycles of: (92°C, 30 s; ramp 0.5C/s to 55°C 55°C, 30s, ramp 0.5C/s to 72°C; 72°C, 30 s) 72°C, 10 min	~200bp **WT** or **Spd** 181 bp **Δ5** (this reaction does not distinguish between WT and Spd alleles)
Sex	**Forward:** TGAAGCTTTTGGCTTTGAG **Reverse:** CCGCTGCCAAATTCTTTGG	94°C, 5 min; 30 cycles of: (94°C, 30 s; 55°C, 30 s; 72°C, 30 s); 72°C, 10 min	Single band 350bp = **Female** Double bands 320 and 350 bp = **Male**

Table 2:

Primary and Secondary Antibodies Used in Immunohistochemical Analysis

Antigen	Host	Supplier	Catalog No.; RRID	Dilution
Hu C/D	Human	Gift of V. Lennon	N/A; AB_2813895	1:10,000
Ki67	Rabbit	Abcam	ab15580; AB_443209	1:1,000
β-III Tubulin (aka TuJ1, Tubb3)	Rabbit	Covance	PRB-435P AB_291637	1:10,000
PECAM (CD31)	Rat	Abcam	ab28364; AB_726362	1:500
Calcitonin Gene Related Peptide (CGRP)	Rabbit	Sigma Aldrich	C8198; AB_259091	1:1,000
Tyrosine Hydroxylase	Sheep	Millipore	AB1542; AB_90755	1:1,000

Secondary Antibody	Fluorophore	Supplier	Catalog No.; RRID	Dilution
Donkey anti-Human	Cy3	Jackson ImmunoResearch	709-165-149; AB_2340535	1:1,600
Donkey anti-Human	Cy5	Jackson ImmunoResearch	709-605-149; AB_2340578	1:250
Donkey anti-Rabbit	Alexa 488	Jackson ImmunoResearch	711-545-152; AB_2313584	1:400
Donkey anti-Rabbit	Cy5	Jackson ImmunoResearch	711-175-152 AB_2340607	1:250
Donkey anti-Sheep	Alexa 488	Jackson ImmunoResearch	713-545-147; AB_2340745	1:400
Donkey anti-Rat	Cy5	Jackson ImmunoResearch	712-175-150; AB_2340671	1:250

Abbreviations: N/A, not applicable; RRID, Research Resource Identifier